NeuroImage **16,** 217–240 (2002)
doi:10.1006/nimg.2001.1054, available online at http://www.idealibrary.com on IDEAL®

Image Distortion Correction in fMRI: A Quantitative Evaluation

Chloe Hutton, Andreas Bork, Oliver Josephs, Ralf Deichmann, John Ashburner, and Robert Turner

Wellcome Department of Cognitive Neurology, Institute of Neurology, London WCIN 3BG, United Kingdom

Received July 11, 2001

A well-recognized problem with the echo-planar imaging (EPI) technique most commonly used for functional magnetic resonance imaging (fMRI) studies is geometric distortion caused by magnetic field inhomogeneity. This makes it difficult to achieve an accurate registration between a functional activation map calculated from an EPI time series and an undistorted, high resolution anatomical image. A correction method based on mapping the spatial distribution of field inhomogeneities can be used to reduce these distortions. This approach is attractive in its simplicity but requires postprocessing to improve the robustness of the acquired field map and reduce any secondary artifacts. Furthermore, the distribution of the internal magnetic field throughout the head is position dependent resulting in an interaction between distortion and head motion. Therefore, a single field map may not be sufficient to correct for the distortions throughout a whole fMRI time series. In this paper we present a quantitative evaluation of image distortion correction for fMRI at 2T. We assess (i) methods for the acquisition and calculation of field maps, (ii) the effect of image distortion correction on the coregistration between anatomical and functional images, and (iii) the interaction between distortion and head motion, assessing the feasibility of using field maps to reduce this effect. We propose that field maps with acceptable noise levels can be generated easily using a dual echo-time EPI sequence and demonstrate the importance of distortion correction for anatomical coregistration, even for small distortions. Using a dual echo-time series to generate a unique field map at each time point, we characterize the interaction between head motion and geometric distortion. However, we suggest that the variance between successively measured field maps introduces additional unwanted variance in the voxel time-series and is therefore not adequate to correct for time-varying distortions.

INTRODUCTION

Echo-planar imaging (EPI) with gradient echo is currently used almost universally for functional neuroimaging studies. It is possible to acquire whole brain images with high signal-to-noise ratio in a matter of seconds. The main limitation of this method is its sensitivity to magnetic field inhomogeneity. In regions where the magnetic field varies, voxels are shifted from their correct positions and may be compressed or stretched so that the voxel brightness, which is proportional to the volume to which it corresponds, is altered (Schmitt *et al.,* 1998). These effects result in geometric distortion and intensity nonuniformity, well-recognized problems with EPI (Weisskoff and Davis, 1992; Bowtell *et al.,* 1994; Jezzard and Balaban, 1995). Sources of field inhomogeneity are poor shimming and differing susceptibilities of neighbouring tissues. The latter effect is most severe in regions where air-filled sinuses border with bone or tissue such as the frontal lobes and temporal lobes, but is also apparent to a lesser extent in other regions. When the field inhomogeneity is large enough, the signal in that region is lost all together. This susceptibility-induced signal loss is a related artefact that currently limits the use of EPI for tasks involving regions in the temporal and frontal lobes (Ojemann *et al.,* 1997; Devlin *et al.,* 2000; Gorno-Tempini *et al.,* 2001). This paper focuses on the correction of moderate geometric distortion.

One of the main consequences of geometric distortion is that it is difficult to achieve an accurate registration between an activation map calculated from an fMRI time series and an undistorted high resolution anatomical image. This is important for the anatomical localisation of functional activations in which a mismatch of 1 or 2 voxels (up to 6 mm) can lead to misinterpretation of the results. Accurate registration is of particular importance when anatomical information is being exploited in the analysis of fMRI data. For example the cortical surface can be manipulated to provide an alternative coordinate system for functional activations (Van Essen and Drury, 1997; Fischl *et al.,* 1999) or can be explicitly used for surface-based fMRI analyses (Kiebel *et al.,* 2000; Andrade *et al.,* 2000).

Reducing magnetic field inhomogeneities decreases geometric distortion. This can be achieved by optimising the shim and many MRI scanners now have software to do this quickly and automatically. However, the inhomogeneity arising from tissues with different

1053-8119/02 $35.00

susceptibilities can be shimmed only by using localised shimming methods similar to those used in spectroscopy (Mao and Kidambi, 2000). This approach may be advantageous for focussing on a single part of the brain but can cause severe distortions in the rest of the brain and may still not be able to correct for the large variations in magnetic field occurring in some regions.

Different techniques to correct for image distortion have been reported. Mostly these methods involve the acquisition of field maps representing the field inhomogeneity across the images. These maps are used to correct the distorted images in a postprocessing step (Weisskoff and Davis, 1992; Jezzard and Balaban, 1995; Reber *et al.*, 1999; Chen *et al.*, 2000). In other methods, bipolar field gradient images have been used to generate the distortion correction (Bowtell *et al.*, 1994) and a multireference scan used to correct for distortion during image reconstruction (Wan *et al.*, 1995). In this paper we are concerned with postprocessing correction methods that are based on the computation of a field map from gradient-recalled images with different echo-times (Weisskoff and Davis, 1992; Jezzard and Balaban, 1995). A field map can be computed from the phase of the complex image data. By collecting more than one echo spaced in time it is possible to measure changes in the phase (and therefore the magnetic field) that are independent of imaging gradients and artefacts caused by the excitation pulse. Image processing techniques are required to convert the phase change map into a map of voxel shifts that can then be used to unwarp the distorted images. In this paper we present a quantitative evaluation of this field map based distortion correction for fMRI at 2T. We use a method based on that of Jezzard and Balaban (1995). Our approach differs in that we use dual echo-time EPI data to generate the field map. This can be acquired quickly and has the same geometric properties as the distorted functional images. We demonstrate that an optimal echo-time difference can be selected for acquiring the field map. We assess the effect of distortion correction on the registration between functional and anatomical images using a measure of mutual information.

The distortion correction methods described above assume that there is no head motion between acquisitions of the field map and the distorted EPI data. Although it is possible to register the field map with the EPI data, the distribution of the magnetic field throughout the head is position dependent and it has been demonstrated that the distortions vary with head motion (Jezzard and Clare, 1999). This means that a single field map acquired at the beginning of an fMRI scanning session will not necessarily represent the distortions in all of the acquired images. The field inhomogeneity can be considered as having a static component that affects every image and can be represented by a single field map and a time-varying component that varies with head motion. The static component can be corrected with a single field map while the time-varying component will remain as a source of variance in the time series even after the images have been realigned and distortion corrected. We therefore use a dual echo-time sequence to acquire fMRI time-series with two EPI images at each time point. The two images have different echo-times so that a robust field map can be calculated at each time point. This allows us to measure unique, position-specific field maps and to assess the variation in distortion with head movement. Jezzard and Clare (1999) demonstrated that at 3T, movements of the order of 5 degrees give rise to distortion changes of the order of 2 to 3 voxels. In general our findings agree with this report (although the distortions are slightly smaller over the whole brain because our experiments have been carried out at 2T). We also investigated smaller, more typically sized head movements and show that the interaction between head motion and distortion is of a similar scale to the variance between successively measured field maps. The error introduced by successive field map differences will therefore manifest itself as an increase the variance of voxel time-series (i.e., temporal noise). For this reason we suggest that a uniquely calculated field map for each image in an fMRI time-series generates too much temporal noise to usefully correct for time-varying distortions.

THEORY

The phase evolution of a voxel in an MR image depends on the local magnetic field that it has experienced since the excitation pulse. The field of view (FOV) and therefore spatial localisation of signal is controlled by magnetic field gradients in the three image dimensions. Where local field inhomogeneities add to the deliberate imaging gradients there is a miscalculation of the local FOV leading to spatial distortion. This effect is coupled with changes in image intensity. The amount of local distortion is therefore proportional to the absolute value of the field inhomogeneity and the data acquisition time. Distortion caused by susceptibility effects also increases with magnetic field strength.

EPI is particularly sensitive to the effects of magnetic field inhomogeneities because it has relatively long total readout times. In contrast to other MRI techniques that acquire a single line of raw data after each excitation pulse, with EPI a whole slice of raw data is acquired after a single excitation pulse. The time between the collection of adjacent k-space points can differ substantially between the two dimensions. The result is that distortions arise in the direction in which the acquisition time between adjacent points is greatest. This is the phase-encoding direction, which is often associated with the anterior-posterior axis in the MR image of the brain and will be referred to here as

the y-axis. Distortions in the orthogonal direction (the read-out direction often associated with the right-left axis) are negligible because the acquisition time between adjacent points along this axis is much less. Correcting for distortions in EPI therefore involves repositioning voxels in one dimension of the image only.

To generate a map of the one-dimensional image distortions, it is necessary to collect a map of the field inhomogeneity $\Delta B_0(x, y, z)$ (or a field map) where (x, y, z) correspond to voxel coordinates in the image. This can be calculated from a map of the phase evolution of each voxel using

$$\Delta B_0(x, y, z) = (2\pi\gamma\Delta TE)^{-1}\Delta\Theta(x, y, z), \qquad (1)$$

where ΔB_0 (x, y, z) is measured in Hz, $\Delta\Theta(x, y, z)$ is the phase evolution measured over time ΔTE and γ is the gyromagnetic ratio (Jezzard and Balaban, 1995).

Phase information can be directly accessed from the complex data of an MR image. This information represents the phase evolution over the echo-time. If the phase information is extracted from the difference of two echoes with an echo-time offset, it is possible to eliminate unwanted effects that are common to both images. In this case, in equation 1, $\Delta\Theta(x, y, z)$ is the phase difference between the two echoes and ΔTE is the echo-time difference. The phase difference map can therefore be scaled to represent the measured field inhomogeneity and then converted into a map of one-dimensional voxel shifts along the y-axis by multiplying the field map by the acquisition time,

$$d_y(x, y, z) = \gamma\Delta B_0(x, y, z)T_{acq}, \qquad (2)$$

where T_{acq} is the readout time for a slice of raw data, d_y is the map of one-dimensional voxel shifts in the y-axis. If EPI is used to acquire the phase information, the map of voxel shifts will be in distorted space such that a voxel with coordinates (x, y, z) in the distorted image has been shifted by $d_y(x, y, z)$. The map of one-dimensional shifts, $d_y(x, y, z)$ can be considered as the warp field in distorted image space that describes the mapping from points in an undistorted image to points in the distorted image. To estimate the undistorted image from the distorted image, we must find the warp field that maps from points in the distorted space to points in the undistorted space. This requires the calculation of the inverse transformation $d_{y'}(x, y', z)$, where y' is the y-coordinate in undistorted space corresponding to y in the distorted image space.

We find $d_{y'}(x, y', z)$ by first assuming that the field map can be represented by a set of piecewise one-dimensional linear functions. Each piecewise linear function in the distorted image space can then be calculated for points in the undistorted image space using linear interpolation. We use the map of voxel shifts in undistorted image space, $d_{y'}(x, y', z)$ to sample the points in the distorted image and create the undistorted image,

$$I_{\text{undistorted}}(x, y', z) = I_{\text{distorted}}(x, y' + d_{y'}(x, y', z), z). \qquad (3)$$

This step requires interpolation to account for sub-voxel shifts in the voxel shift map.

As described previously, geometric distortion is accompanied by compression or stretching of voxels so that the voxel brightness is altered as well as voxel position. We apply an adjustment based on the one described by Jezzard and Balaban (1995), which uses the one-dimensional derivative of the map of voxel shifts in undistorted space in the phase-encoding direction. This gives a measure of the local voxel shift gradient at each voxel which, when applied to the undistorted image has the effect of decreasing voxel brightness values that were increased by the distortion and vice-versa. The undistorted image is multiplied by one minus the one-dimensional derivative of the voxel shift map in undistorted image space to perform the intensity adjustment,

$$I^{\text{intensity-corr}}_{\text{undistorted}}(x, y', z) = (1 - \delta(d_{y'}(x, y', z)/\delta y'))I_{\text{undistorted}}(x, y', z). \qquad (4)$$

The one-dimensional derivative in the phase-encoding direction is calculated discretely using,

$$\delta(d_{y'}(x, y', z))/\delta y' = \frac{1}{2}[d_{y'}(x, y' + 1, z) - d_{y'}(x, y' - 1, z)]. \qquad (5)$$

One of the greatest limitations of EPI occurs when a local field gradient causes a phase change of about 2π or more across a voxel. In this case the signal from that voxel is not displaced but lost all together due to signal dephasing. It is not possible to correct for susceptibility induced signal loss using field mapping techniques.

ACQUISITION AND CALCULATION OF FIELD MAPS

Different procedures for the acquisition and calculation of field maps have been presented in the literature. The acquisition strategy can be optimized in terms of the extra time involved in acquiring the field map and the robustness of the calculated voxel shift map.

Acquisition Time

In the course of an fMRI study it may take 10 to 15 min to acquire a high resolution anatomical scan and

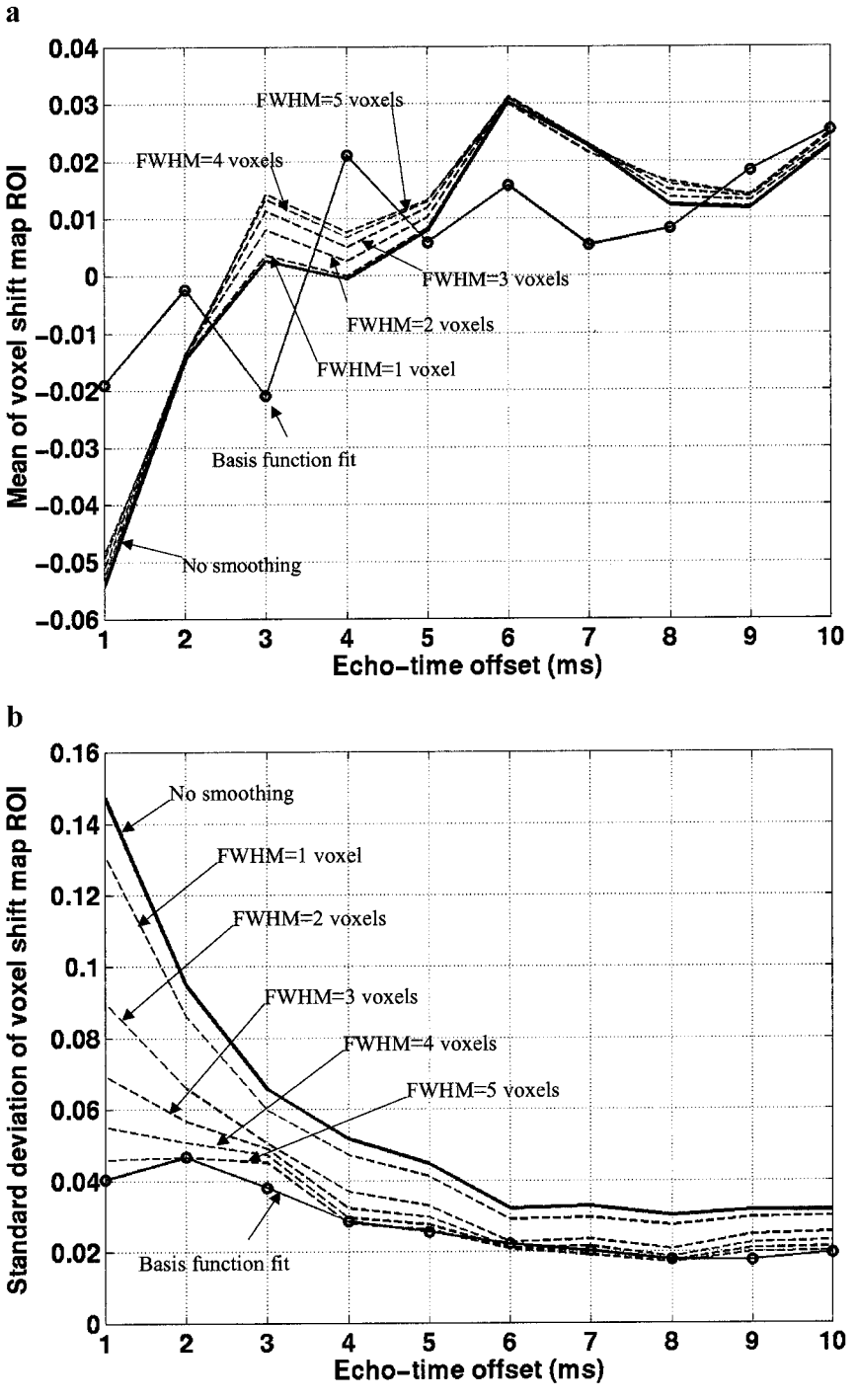

FIG. 1. (a) The solid line shows the mean signal level within a region of interest of the voxel shift maps calculated for different echo-time offsets. The region of interest corresponds to a homogeneous region of the magnetic field. Each of the dashed lines shows the mean signal level within the same region of interest after the voxel shift maps have been smoothed. Each line represents a different amount of Gaussian smoothing plotted against echo-time offsets. The line joined with circles shows the mean signal level within the same region of interest of a voxel shift map generated by fitting a set of discrete cosine basis functions to the original field map. The mean value in a homogeneous region of the field should be approximately zero, but the plots show that the deviation from zero (due to measurement noise) is greatest for shorter echo-time differences. (b) The solid line shows the standard deviation within a homogeneous region of interest of voxel shift maps calculated for different echo-time offsets and illustrates the decrease in standard deviation as echo-time offset increases. The dashed lines show the standard deviation within the same region of interest of the voxel shift maps calculated using different echo-time offsets and with different amounts of smoothing. The line joined with circles shows the standard deviation within the same region of interest of a voxel shift map generated by fitting a set of discrete cosine basis functions to the original field map. The dashed lines illustrate that not surprisingly, the standard deviation is decreased with smoothing (the FWHM of the Gaussian smoothing kernel was

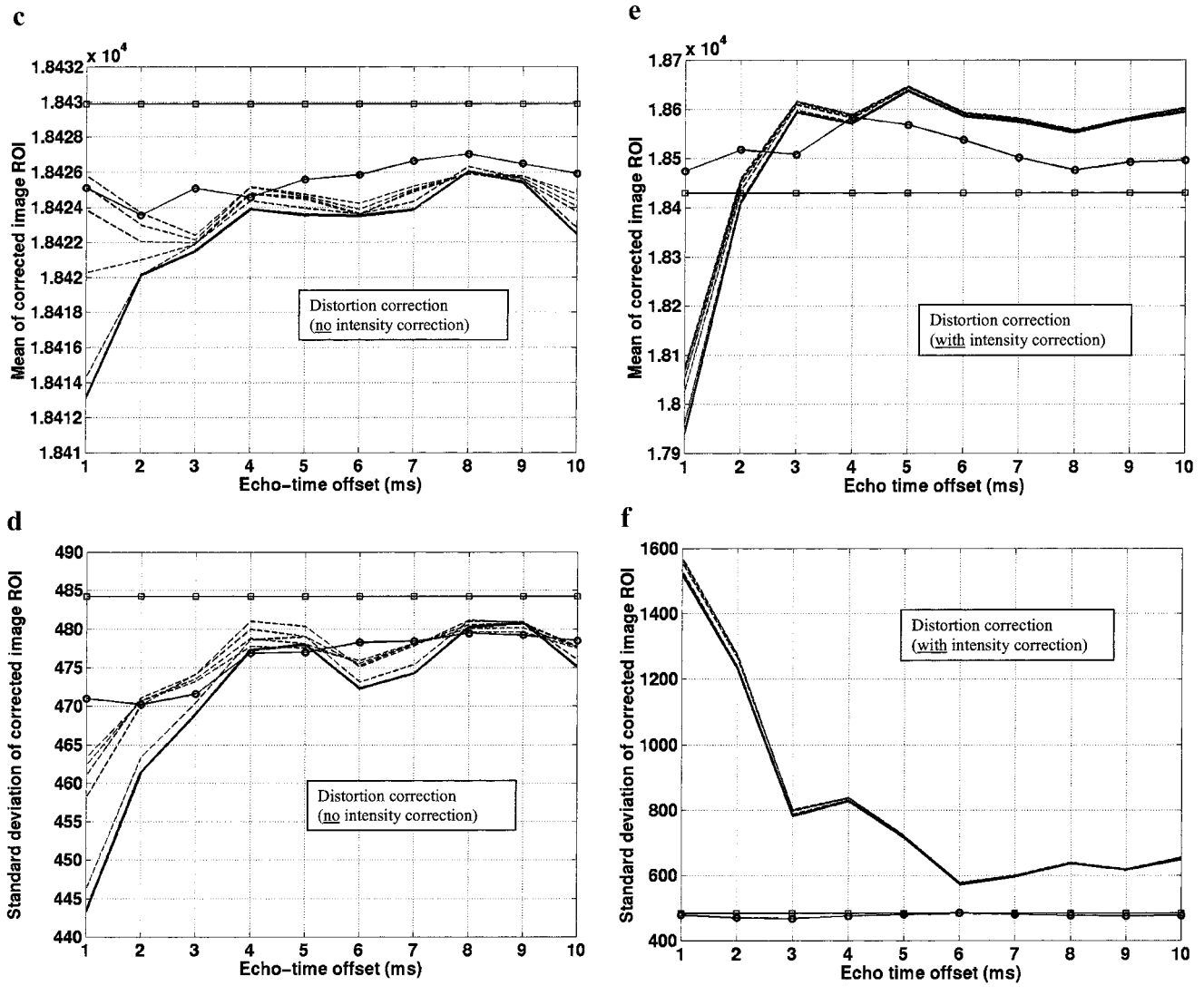

FIG. 1—*Continued*

20 min or more to acquire an fMRI time series of T2*-weighted images. The time taken to acquire any additional scans should therefore be kept to a minimum. A field map based on the acquisition of two EPI volumes has certain advantages. First, it takes just a matter of seconds to acquire. Second, minimizing the

increased from 1 to 5 voxels in unit steps). However, there is a much smaller reduction in standard deviation due to smoothing for field maps acquired with longer compared with shorter echo-time offsets. (c) Mean image intensity versus echo-time offset within a homogeneous region of interest after distortion correction with no intensity correction. The plots show the mean of the image intensity after distortion correction with the unsmoothed voxel shift map (solid line), with an increasingly smoothed field map (dashed lines), and with the DCT basis function fit (line joined by circles). The straight line joined by squares represents the mean of the original distorted image. (d) Standard deviation of image intensity versus echo-time offset within a homogeneous region of interest after distortion correction with no intensity correction. The plots show the standard deviation of the image intensity after distortion correction with the unsmoothed voxel shift map (solid line), with an increasingly smoothed field map (dashed lines), and with the DCT basis function fit (line joined by circles). The straight line joined by squares represents the standard deviation of the original distorted image. (e) Mean image intensity versus echo-time offset within a homogeneous region of interest after distortion correction with intensity correction. The plots show the mean of the image intensity after distortion correction and intensity correction with the unsmoothed voxel shift map (solid line), with an increasingly smoothed field map (dashed lines), and with the DCT basis function fit (line joined by circles). The straight line joined by squares represents the mean of the original distorted image. (f) Standard deviation of image intensity versus echo-time offset within a homogeneous region of interest after distortion correction with intensity correction. The plots show the standard deviation of the image intensity after distortion correction and intensity correction with the unsmoothed voxel shift map (solid line), with an increasingly smoothed field map (dashed lines), and with the DCT basis function fit (line joined by circles). The straight line joined by squares represents the standard deviation of the original distorted image.

time taken to acquire the two echoes reduces the possibility of artefact due to motion. Finally, the EPI field map will have the same geometric characteristics as the fMRI data so that unwarping the images involves minimal processing and linear registration with the EPI data before repositioning voxels along one dimension of the image using linear interpolation.

Decreasing Field Map Noise

As described in Eqs. (1) to (3) above, distortion correction involves scaling the field map, converting it into voxel shifts that describe the mapping from distorted to undistorted space, then using it to sample the correct points forming the undistorted image. Noise in the calculated field map will therefore introduce spatial errors in the undistorted images. In a region of the image where the magnetic field is uniform, (i.e., $\Delta B_0(x, y, z) = 0$), there should be no change in position of the voxels in the corresponding image. However, the measured field will have measurement noise so that the position of a voxel in the corrected image will be determined by the field values in the corresponding local voxel neighbourhood. Interpolation is required to calculate the intensity of voxels after adjusting their position so that the resulting intensities will also be dependent on field map noise. It is therefore important to minimize noise in the field map, which can be achieved with the correct choice of acquisition parameters and with spatial smoothing.

Increasing the echo-time difference of the two images used to calculate the field map increases the signal-to-noise ratio in the acquired phase maps. For fMRI studies, EPI echo-time is usually selected to maximise BOLD sensitivity and reduce susceptibility-induced signal loss (Bandettini *et al.*, 1994; Jesmanowicz *et al.*, 1999). Therefore, if the optimal echo-time is used to acquire the first, longer echo in the field map acquisition, then the second echo-time should be as short as possible for two reasons. First, the shorter echo will have less susceptibility-induced signal loss and secondly the echo-time difference will be maximized. This is better than increasing the echo-time difference by increasing the longer echo-time because the increased noise in longer echo-time images would dominate the noise in the calculated field map.

Different regularisation methods for smoothing field maps have been compared by other authors and the results suggest that Gaussian smoothing provides the best regularised field map for distortion correction (Jenkinson, 2001). In this work we wanted to assess the effect of echo-time difference and spatial smoothing on the signal variance (i.e., noise) in a field map based on an EPI sequence. We carried out the following experiments using a gel phantom. Multislice GE EPI images were acquired on a Siemens Vision 2T scanner with matrix size = 64 × 64, FOV = 192 cm, slice thickness of 1.8 mm with a 1.2-mm gap, TR per slice = 76 ms, and 32 slices. A series of EPI images were collected with echo-times ranging from 40 to 30 ms in steps of 1 ms. A field map was calculated from pairs of images for which the longer echo-time was always 40 ms and the shorter echo-time was decreased from 39 to 30 ms (in 1-ms steps). Field maps were therefore calculated with echo-time differences ranging from 1 ms to 10 ms (in 1 ms steps). The field maps were scaled as described in Eqs. (1) and (2) and then converted into the voxel shift maps required for distortion correction as described in Eq. (3). We use the terms field map and voxel shift map interchangeably, although in the context of distortion correction, it is practical to consider the field in units of voxel shifts.

We defined a square region of interest (6 × 6 voxels in one slice) within a homogeneous region of the field map. The mean and standard deviation within the region of interest were calculated for each of the voxel shift maps (i.e., those calculated with different echo-time offsets) and are illustrated by the solid lines in Figs. 1a and 1b, respectively. The mean value in a homogeneous region of the field should be approximately zero, but the plots show that the deviation from zero (due to measurement noise) is greatest for the shorter echo-time difference (<0.06 voxels). The standard deviation within the region of interest decreases as the echo-time difference increases (<0.05 voxels).

Figures 1a and 1b also illustrate the effect of gaussian smoothing on noise within a homogeneous region of the field map. The voxel shift map calculated for each echo-time difference was smoothed with a three-dimensional Gaussian filter of increasing kernel size. The full width at half-maximum height (FWHM) of the kernel was increased from 1 to 5 voxels in unit steps. The mean and standard deviation of the smoothed field within the same region of interest as above was measured for the range of smoothing kernels and echo-time offsets. The dashed lines in Fig. 1a show that smoothing does not have a particularly interesting effect on the mean value within the homogeneous region of the field map. Each of the dashed lines in Fig. 1b illustrates that not surprisingly, the standard deviation decreases as the smoothing increases. However, there is a smaller reduction in standard deviation due to smoothing for field maps acquired with longer compared with shorter echo-time offsets. Smoothing is therefore more important for field maps acquired with shorter echo-time offsets.

It is also possible to generate a smoothed version of the field map by fitting to it a smoothly varying function. This is particularly advantageous for modelling field inhomogeneity over the brain because it allows the field to be estimated in regions where low signal-to-noise ratio means that the field cannot be accurately measured. The magnetic field varies smoothly over most regions of the brain but can change more rapidly

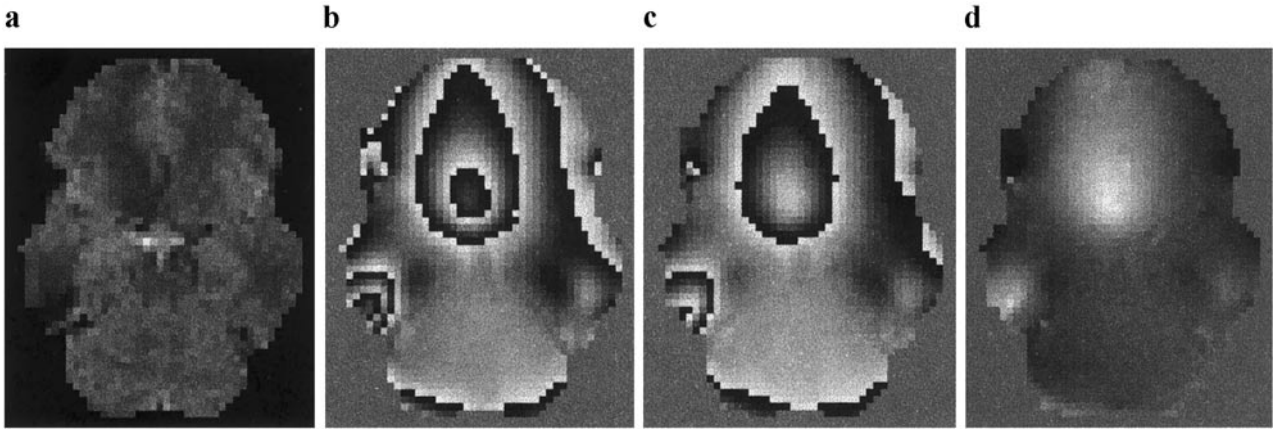

FIG. 2. Phase unwrapping of dual echo-time EPI data. (a) Slice through EPI volume. (b) Corresponding slice through wrapped phase map acquired with longer echo-time. (c) Corresponding slice through wrapped phase map acquired with shorter echo-time. This slice has fewer discontinuities compared with the longer echo time. (d) Ratio of the two complex images acquired with an echo-time offset of 10 ms. Discontinuities due to phase wrapping cancel out. All of the phase images have been masked with a thresholded version of the intensity image.

in regions affected by susceptibility artefacts. To model these characteristics of the field, Jezzard and Balaban (1995), fit a 2-D polynomial surface to the field map. In this work we fit a linear combination of low frequency basis functions to the field map. We use the eight lowest frequency basis functions (including the constant, linear component) of the three-dimensional discrete cosine set of transformations (DCT; Jain, 1989) to model each spatial dimension. The field is therefore modelled by a total of 512 (8^3) basis functions. This number of basis functions in three dimensions has been chosen empirically for brain images and allows rapid changes in the magnetic field to be modeled without over-fitting to noise or errors in the measured phase map. Although the DCT basis function model is fitted to the phantom data in this section, the significance of using this smoothing method for brain images will become apparent in the following section.

To observe the smoothing effect of the DCT basis function model versus echo-time difference, the model was fitted to the phantom field maps calculated above. The mean and standard deviation of the modeled field map was calculated within the same region of interest and the results are illustrated by the lines joined with circles in Figs. 1a and 1b, respectively. The mean of the modeled field map deviates from zero, although less than the original and smoothed field maps for shorter echo-time offsets. At longer echo-time offsets the mean of the modeled field map varies from the original and smoothed field maps by less than 0.005 voxels. The standard deviation of the modeled field map is slightly smaller than that of the original and smoothed field maps.

We used the field maps calculated in the previous steps to distortion correct the original 40-ms echo-time image as described in Eq. (3). Field maps before and after both gaussian smoothing and DCT basis function fitting were used for distortion correction to observe how smoothing the field map influences the corrected image intensities. Distortion correction was applied both with and without the intensity correction described by Eqs. (4) and (5).

The mean and standard deviation of the distortion-corrected image intensities with and without intensity correction were measured within the same region of interest as above. Plots of the mean and standard deviation versus echo-time offset are shown for distortion correction without intensity correction in Figs. 1c and 1d, respectively, and with intensity correction in Figs. 1e and 1f, respectively. Each figure shows the mean or standard deviation of the image intensity after distortion correction with the unsmoothed voxel shift map (solid line), with an increasingly gaussian smoothed field map (dashed lines), and with the DCT basis function fit (line joined by circles). In each figure, the straight line joined by squares represents the mean or standard deviation of the original distorted image.

The results without intensity correction (Figs. 1c and 1d) show that both the mean and standard deviation of the original image are decreased by all methods of distortion correction. For short echo-time offsets this decrease is quite abrupt. The mean and standard deviation are reduced because the distortion correction itself has a smoothing effect on the image. This is caused by the interpolation required for the sub-voxel shifts from distorted to undistorted positions [Eq. (3)]. The noisier the voxel shift map, the more subvoxel shifting is required for the distortion correction resulting in a smoother distortion-corrected image. At echo times longer than 3 ms, there appears to be very little difference between the results for the different methods of distortion correction without intensity correction.

The distortion correction results with intensity correction (Figs. 1e and 1f) show that the mean of the original image is increased by all correction methods

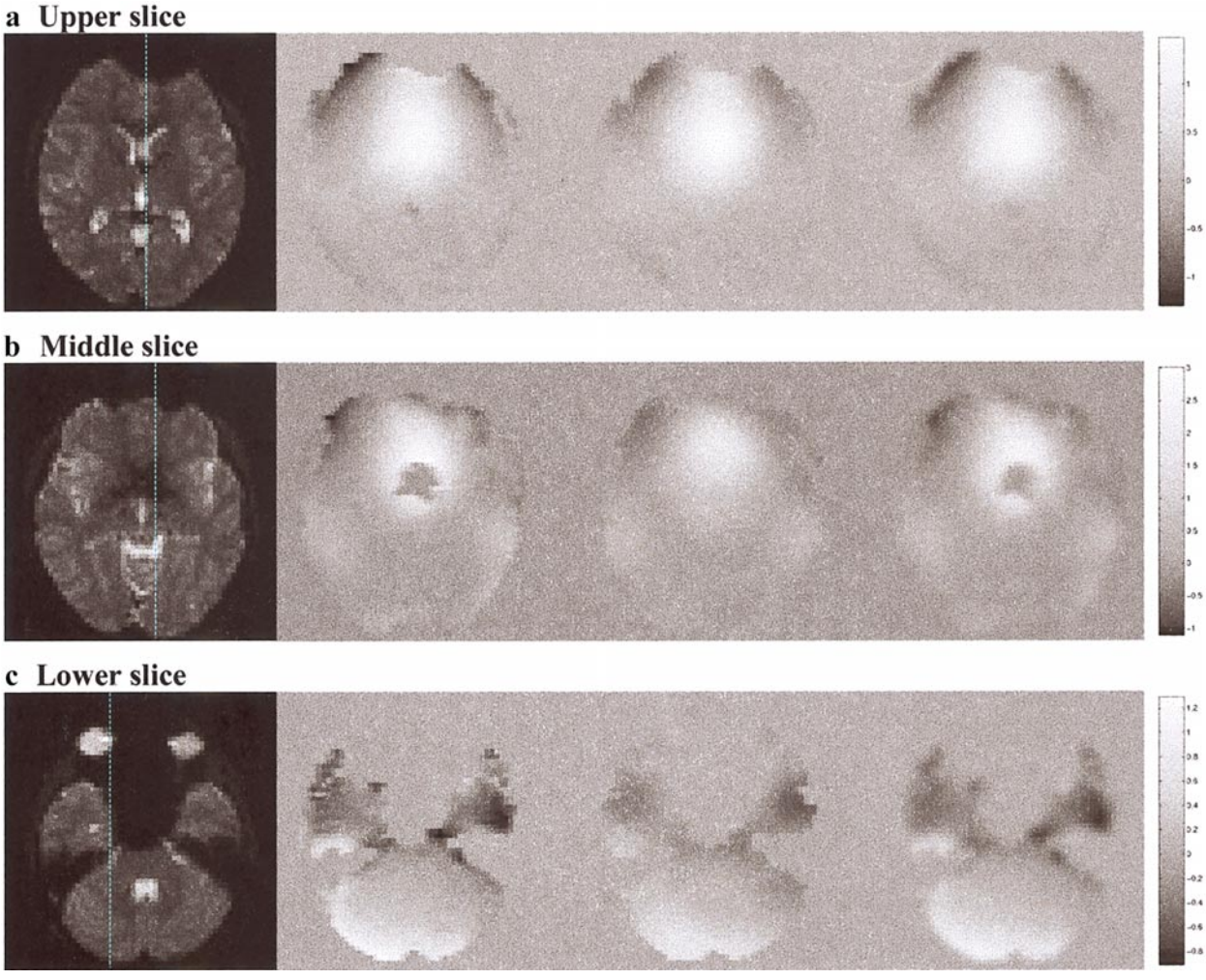

FIG. 3. (a–c) Each row contains a slice from the intensity image (left) corresponding to a low-noise mean field map (second column), the basis function fit to the mean field map (third column), and the gaussian smoothed (FWHM = 1 voxel) mean field map (right) for (a) an upper slice, (b) a middle slice, and (c) a lower slice in the brain. The dashed lines through the intensity image slices represent the position of the profiles through the corresponding field maps, which are plotted in d–f. (d–f) Profiles through the field maps shown in a–c, respectively. The solid line is a plot of the profile through the mean field map. The dashed lines are plots through the mean field map after increased levels of gaussian smoothing (FWHM = 1 to 5 voxels). The line joined with circles is a plot through the basis function fit to the mean field map.

for echo-time offsets greater than 2 ms. The standard deviation of the original image is increased by all methods of distortion correction except for the DCT basis function fit. These results suggest that including an intensity correction may increase the noise in the corrected image. As described in Eqs. (4) and (5), the intensity correction is based on a function of the one-dimensional derivative of the voxel shift map, which is multiplied by the image intensity. Therefore, if the voxel shift map is noisy it is clear that this will result in an increase in image noise. The DCT basis function fit is very smooth and therefore an intensity correction based on its derivative introduces less image noise.

Phase Unwrapping

The robustness of the calculated field map is dependent not only on the noise characteristics of the acquired phase maps but also on the ability to extract reliable phase information from the measured complex data. The problem is that phase is uniquely defined only in the principal value range of $[-\pi, \pi]$. Any value outside this range will be wrapped around so that its so-called "wrapped phase" is offset from its actual phase by an integer multiple of 2π. Phase wrapping can be detected as spatial discontinuities in the phase map and can be "unwrapped" by adding or subtracting multiples of 2π to the voxels where these discontinuities occur. The addition and subtraction of multiples of 2π can be arbitrary over the image. It is therefore important to correctly define where in the image the "wrapped phase" offset is zero. This can be achieved by defining a starting point for the phase unwrapping that corresponds to the most uniform region of the magnetic field, i.e., where the field should be approximately zero.

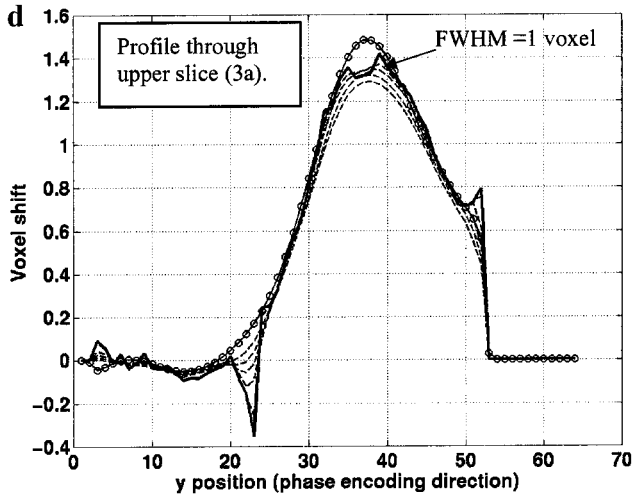

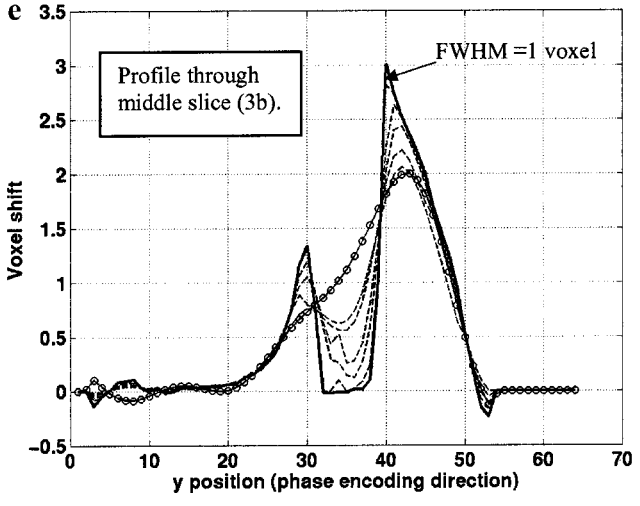

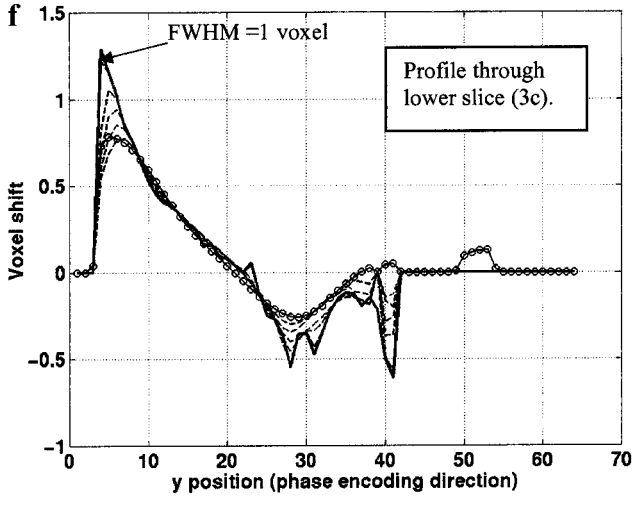

FIG. 3—*Continued*

Discontinuities due to phase wrapping can be minimised by computing the phase map from the ratio of two complex images acquired with different echo-times. This is equivalent to finding the difference between the two phase components of the complex images (i.e., the phase evolution between the two echo-times). If the time between the two echoes is not too long, the phase offset of many of the "phase wrapped" voxels will be the same in the two echoes and will cancel out in the ratio of the two complex images. This will reduce the number of voxels that require phase unwrapping or eliminate them altogether. However, as shown in the previous section, a longer echo-time offset yields improved signal-to-noise in the measured field map. Therefore a trade-off must be found between these two factors. Figure 2 illustrates the calculation of a phase map using a dual echo-time EPI acquired with a 10-ms offset. The figure shows that no phase unwrapping is necessary once the ratio of the two complex images has been computed.

Even with minimal phase discontinuities, phase unwrapping algorithms may not be completely robust when applied to noisy three-dimensional EPI data. EPI images of the brain present specific difficulties because of the brain anatomy and susceptibility artefacts. In general, phase unwrapping algorithms use the condition that the phase difference between adjacent voxels should be less than π radians (Axel and Morton, 1989; Hedly and Rosenfeld, 1992). This condition is sensitive to noise and is particularly a problem in regions of low signal intensity. It is also dependent on spatial continuity across the object within the image. Phase unwrapping is usually reliable in the upper slices of the brain, where there are spatially continuous regions within each slice. In the lower slices of the brain where regions appear to be spatially disconnected, either because of the anatomy of that region or susceptibility induced signal loss, phase unwrapping is less reliable. More sophisticated approaches to phase-unwrapping have been proposed (Cusack *et al.*, 1995, 2001), which may provide improved results in the presence of discontinuities caused by noise. In general many unwrapping algorithms are not completely fail-safe and require some heuristic measures to ensure that the final field map does not contain any errors.

Creating a Field Map of the Brain

We describe a method for generating field maps of the brain that has been applied successfully in this work. Voxels must be spatially connected for successful phase unwrapping. Therefore we create an intensity mask based on the spatial connectivity of voxels as well as grey level intensity by labelling all voxels above a specified threshold (based on the mean intensity of the image) that are connected with all other voxels in the object. The spatial connectivity mask will contain most of the brain but will exclude regions that appear to be disconnected in the image such as eyeballs and inferior frontal regions. This mask is generated using the

longer echo-time image, which will have the most susceptibility-induced signal loss. Multiplying the phase map by this mask will therefore ensure robust phase unwrapping within spatially connected regions of the brain resulting in an unwrapped phase map that can be scaled and converted to a voxel shift map using Eqs. (1) and (2). The resulting masked field map can be used for distortion correction as described in Eq. (3), but because of anatomy or signal loss some disconnected brain regions or regions with low signal intensity will be excluded from the resulting unwrapped phase map. We therefore fit the DCT basis function model described under "Decreasing field map noise" to this masked field map. Outside of the masked regions the function will vary smoothly and slowly providing an estimation of the phase. We then create a second intensity mask based on a thresholded version of the image acquired at the shorter echo-time which has less susceptibility-induced signal loss (again with the threshold based on the mean image intensity). The second mask is not dependent on spatial connectivity in the brain and is used to identify brain regions that were excluded by the first mask.

By masking the basis function model fit with the second mask we can estimate the phase in regions of the brain excluded by the first mask. There still will be regions of the brain where phase information is missing due to susceptibility induced signal loss. However, as there is no EPI signal in these regions it is only necessary to constrain the modelled phase map to fall smoothly to a value of zero. This is assuming that the phase unwrapping correctly defined the zero offset to correspond to a region where the field inhomogeneity is approximately zero as described under "Phase unwrapping." This is achieved by dilating and smoothing the second mask as described in Jezzard and Balaban (1995). The result provides a model of the field inhomogeneity over the whole brain with minimal noise and errors, which can be converted into a map of voxel shifts and used to unwarp the distorted images.

Decreasing Noise in Field Maps of the Brain

The previous results demonstrate the effect of spatial smoothing within a homogeneous region of a phantom field map. However, the magnetic field within a human brain has more inhomogeneities so that spatial smoothing of the field map may cause artifactual blurring in regions where the field changes rapidly. To investigate this effect, we constructed a low-noise reference field map by acquiring a series of 50 dual echo-time EPI images. Each pair of images had echo-times equal to 40 and 30 ms. All other acquisition parameters were the same as described in the previous section. During the scanning session, the subject remained as still as possible.

An unwrapped phase map was calculated from each pair of EPI images by creating a spatial connectivity mask from a 40 ms echo-time image, masking then unwrapping the phase maps as described under "Creating a field map of the brain." The 40 ms echo-time intensity images were registered using SPM'99 (http://www.fil.ion.ucl.ac.uk). The resulting motion parameters were used to coregister the unwrapped phase maps and create a mean phase map. After scaling using Eqs. (1) and (2), a low-noise mean field (voxel shift) map was generated in which spatial variations were mostly due to real variations in the magnetic field rather than measurement noise. This made it possible to assess any artifactual effects of smoothing, especially in regions of the brain where there are rapid changes in the magnetic field.

The mean field map was smoothed with a three-dimensional Gaussian filter of increasing kernel size (FWHM from 1 to 5 voxels). The DCT basis function model was fitted to the mean field map and an intensity mask based on a 30-ms echo-time image was used to mask the model fit as described under "Creating a field map of the brain." The resulting modeled field map gave an estimation of the field in regions excluded by the original unwrapped phase maps.

Figure 3 shows an upper (a), middle (b), and lower (c) slice from the mean field map (second column), the basis function fit (third column), and the field map after gaussian smoothing with a kernel FWHM = 1 voxel (fourth column). The corresponding intensity image slices are also shown in the first column. Representative profiles in the phase encoding direction through the field maps for the upper, middle, and lower slices are shown in Figs. 3d, 3e, and 3f, respectively. The dashed line on each intensity image in Figs. 1a–1c indicates the position of the corresponding profile for each slice.

The profiles demonstrate that in regions where the field varies slowly, the smoothed and modeled field maps do not deviate from the mean field map. In regions where the field changes rapidly, the field smoothed with a gaussian kernel, FWHM = 1 voxel deviates from the mean field by <0.1 voxels (e.g., at the peak values in Figs. 3d–3f). However, more gaussian smoothing and modelling cause artifactual blurring in regions where the field changes rapidly. The field map smoothed with gaussian FWHM = 5 voxels and the modelled field map can deviate by up to 1 voxel from the mean field map (as shown by the peak in Fig. 3e). It should be noted that regions where the field changes rapidly often correspond to low signal to noise ratio in the image where inaccuracies in the distortion correction are least noticeable.

The advantage of the basis function model is that it can provide an estimation of the field in regions where

it can not be measured. This is demonstrated in the region of the sinus in Fig. 3b and the eyeballs in Fig. 3c.

DISTORTION CORRECTION AND ANATOMICAL COREGISTRATION

Other authors have demonstrated that a significant amount of geometrical distortion due to susceptibility artefacts can be corrected using a field map. In this section we show how even small geometric distortions, on the order of 1 or 2 voxels, can cause a noticeable mismatch between functional and anatomical images. To demonstrate the effect of distortion correction on anatomical coregistration it is necessary to consider the relationship between the EPI image and the anatomical image. If an EPI and an anatomical image from the same subject are free of geometric distortions then it can be assumed that the transformation required to coregister these images will be linear, containing only translations, rotations, and scaling to compensate for differences in voxel size. Therefore the transformation required to match a correctly unwarped EPI image to the corresponding anatomical image should also be a linear transformation. In contrast, the transformation required to match a distorted EPI image with the anatomical image will contain nonlinear terms in the direction of the distortion. A linear registration between an undistorted image and the corresponding anatomical image should therefore result in a better match compared to a linear registration between the distorted image and the anatomical image.

In this work, we used a multimodality coregistration method based on information theory to linearly coregister the distorted and undistorted images to the anatomical image. This coregistration method uses the "mutual information" of the two images as a matching criterion. It is based on the work by Collignon *et al.* (1995) and is implemented in SPM'99 (http://www.fil.ion.ucl.ac.uk). This method maximizes the relative entropy of the joint intensity distribution of two images and provides a quantitative measure (the "entropy correlation coefficient"), representing the degree of interdependence of the two images. This measure can be used to compare the maximized mutual information between the EPI and the anatomical image before and after distortion correction. It therefore provides a measure to determine whether the distorted or the undistorted image better matches the anatomical image.

Methods

The effect of distortion correction on anatomical coregistration is demonstrated for three subjects. Anatomical images with isotropic 1 mm voxel resolution were acquired using a centric-ordered phase-encode MP-RAGE sequence optimised for grey and white matter contrast (Deichmann *et al.*, 2000). Dual echo-time EPI images were acquired using multislice GE EPI with matrix size = 64 × 64, FOV = 192 cm, slice thickness = 1.8 mm with a 1.2-mm gap, TR per slice = 76 ms and 48 slices. Two images were acquired with different echo-times of TE = 40 ms and TE = 27 ms. Fat suppression was used to reduce the presence of signal from fat in the images. Images were acquired on a Siemens Vision 2T scanner. The EPI images were reconstructed using a novel trajectory-based method that substantially decreases Nyquist ghost artefacts (Josephs *et al.*, 2000).

Unwrapped phase maps were created as described under "Creating a field map of the brain." Field maps were then generated using two processing methods (F1) gaussian smoothing, FWHM = 1 voxel and (F2) fitting with DCT basis functions as described under "Creating a field map of the brain." The smoothed field map (F1) and the modeled field map (F2) were converted into maps of voxel shifts in undistorted image space then used to correct the distorted EPI images acquired with TE = 40 ms using Eq. (3). Both distortion corrections were applied with and without intensity correction (IC) as described by Eqs. (4) and (5), resulting in four corrected EPI images for each subject (corrected using F1, F1 + IC, F2, F2 + IC).

The distorted and each of the corrected EPI images were independently coregistered to the corresponding subject's anatomical image using the 'mutual information' coregistration method implemented in SPM'99 (http://www.fil.ion.ucl.ac.uk). The "entropy correlation coefficient," a measure of the interdependence of the two images was computed for each set of coregistered images. The coregistration was performed for EPI images after distortion correction using F1, F1 + IC, F2, and F2 + IC. Each of the distortion-corrected images was subtracted from the distorted images after coregistration to highlight differences due to the correction.

FIG. 4. Results of anatomical coregistration. Two slices from the brain are shown for each of the three subjects (subject 1, a and b; subject 2, c and d; subject 3, e and f). (Column I) Subtraction of the corrected EPI image using F1 + IC from the original distorted EPI image. The bright regions indicate where signal in the distorted image is greater than the corrected image and dark regions the opposite. (Column II) Contours of the coregistered distorted (red) and corrected images (F1, pale blue; F1 + IC, dark blue) overlaid on the anatomical image. (Column III) Contours of the coregistered distorted (red) and corrected images (F2, yellow; F2 + IC, dark blue) overlaid on the anatomical image. (Column IV) Smoothed field map. (Column V) Fitted field map. The grey scale bar indicates the size of the measured distortion in voxels with bright values, indicating distortion toward the top of the page and dark values, indicating distortion toward the bottom of the page.

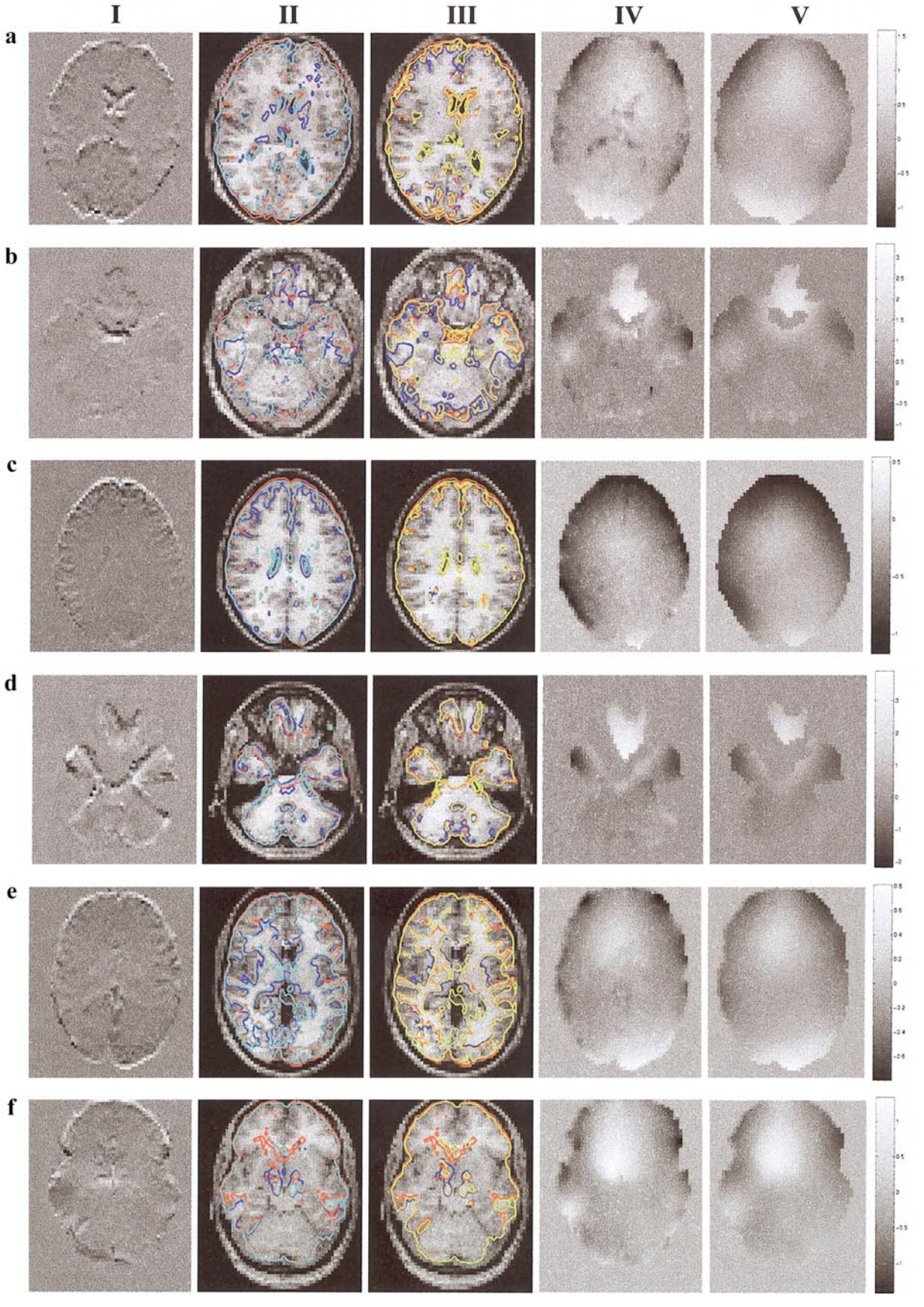

FIGURE 4

Results

The results from the anatomical coregistration are shown in Fig. 4. Two slices from the brain are shown for each of the three subjects (subject 1, a and b; subject 2, c and d; subject 3, e and f). Shown for each subject is a more superior slice in the brain where there are smaller and more typical distortions (a, c, and e) and an inferior slice where the distortion is greatest (b, d, and f). Column I shows the subtraction of the corrected EPI image using F1 + IC from the original distorted EPI image. Bright regions indicate where signal in the distorted image is greater than the corrected image and dark regions the opposite. All the subtraction images for the different correction methods showed a similar pattern of differences. For compactness, only the subtraction results for the F1 + IC correction are shown. These subtraction images indicate where there are differences resulting from the intensity correction as well as the distortion correction. Columns II and III show contours of the distorted and corrected images overlaid on the coregistered anatomical image. The anatomical image has been sampled at the resolution of the EPI images. The contours were calculated using the contour function in Matlab (Matlab 5.3.1, 1999), which draws curves joining together points in the image with the same value. In column II, the red contour corresponds to the distorted EPI image, the pale blue contour corresponds to the corrected image using F1 and the dark blue contour corresponds to the corrected image using F1 + IC. In column III, the red contour again corresponds to the distorted EPI image, the yellow contour corresponds to the corrected image using F2 and the dark blue contour corresponds to the corrected image using F2 + IC. Columns IV and V show the smoothed field map and the fitted field map respectively. The grey scale bar indicates the size of the measured distortion in voxels with bright values indicating distortion towards the top of the page and dark values indicating distortion towards the bottom of the page.

The mismatch between the contours in columns II and III illustrates the mismatch between the distorted and corrected images. In many regions the scale of the mismatch corresponds to the scale of the distortion shown in columns IV and V. In the more superior slices of the brain (a, c, and e), the distortion is of the order of 1 to 1.5 voxels (3–4.5 mm) and causes an apparent stretching of the image slice. The distortion correction appears to work well in such regions. In the more inferior slices where there are more severe susceptibility artefacts (b, d, and e), the scale of the distortion approaches 2–3 voxels (6–9 mm). The maximum distortion occurs in regions where there is almost total signal loss as demonstrated by the contours around the inferior frontal regions in slices b and d. It is therefore difficult to assess the effect of the distortion correction in these regions.

TABLE 1

	Original	F1	F1 + IC	F2	F2 + IC
Subject 1					
Figs. 4a and 4b	0.1925	0.1954	0.1952	0.1964	0.1942
Subject 2					
Figs. 4c and 4d	0.1927	0.1977	0.1999	0.1968	0.1982
Subject 3					
Figs. 4e and 4f	0.2324	0.2359	0.2312	0.2356	0.2310

There are no obvious visible differences in coregistration for the different distortion correction methods (F1 and F2, pale blue and yellow contours in columns II and III, respectively). The difference between distortion correction with and without intensity correction is most apparent in slice b, around the inferior temporal regions.

Coregistration using "mutual information" provides a visibly good match between the anatomical and EPI images (both before and after distortion correction). The Entropy Correlation Coefficients given in Table 1 allow the coregistration of anatomical images to distorted and corrected images to be compared. For all subjects, distortion correction without intensity correction (F1 and F2) improved the coregistration results. In subjects 1 and 2, distortion correction with intensity correction (F1 + IC and F2 + IC) also improved the coregistration results. These results suggest that overall there is a greater level of interdependence and therefore a better match between the functional and anatomical images after distortion correction. Although there was not one method that was consistently better in all data sets, only in subject 1 did the correction method F2 give a better fit than F1 and only in subject 2 was the coregistration improved by intensity correction for both distortion correction methods.

DISTORTION CORRECTION AND HEAD MOTION

Previous work has demonstrated that geometric distortions are modulated by head motion (Jezzard and Clare, 1999). The field inhomogeneity should therefore be considered as having a constant component and a time-varying component due to head motion. The resulting time-varying distortions can be characterized by generating a field map at each time point. We used a dual echo-time EPI sequence that provided two images at each time point. It was therefore possible to calculate a unique field map corresponding to the head position at each time point. This time series allowed us to characterise and evaluate the interaction of distortion with head motion and to test whether the variance introduced by the interaction between distortion and head motion could be removed by distortion correction with a time-varying field map.

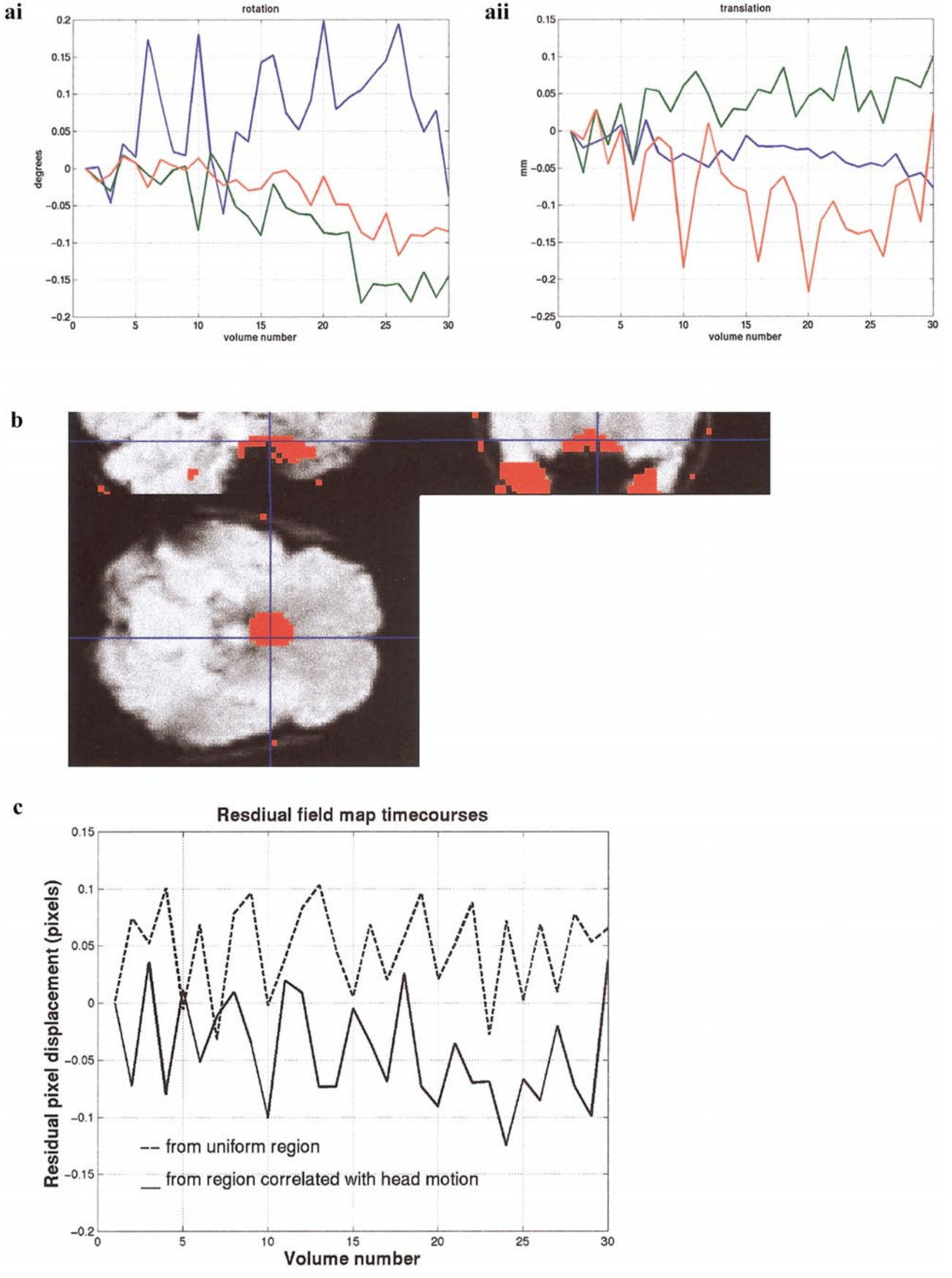
ai
rotation
degrees
volume number
aii
translation
mm
volume number
b
c
Resdiual field map timecourses
Residual pixel displacement (pixels)
-- from uniform region
__ from region correlated with head motion
Volume number

FIGURE 5

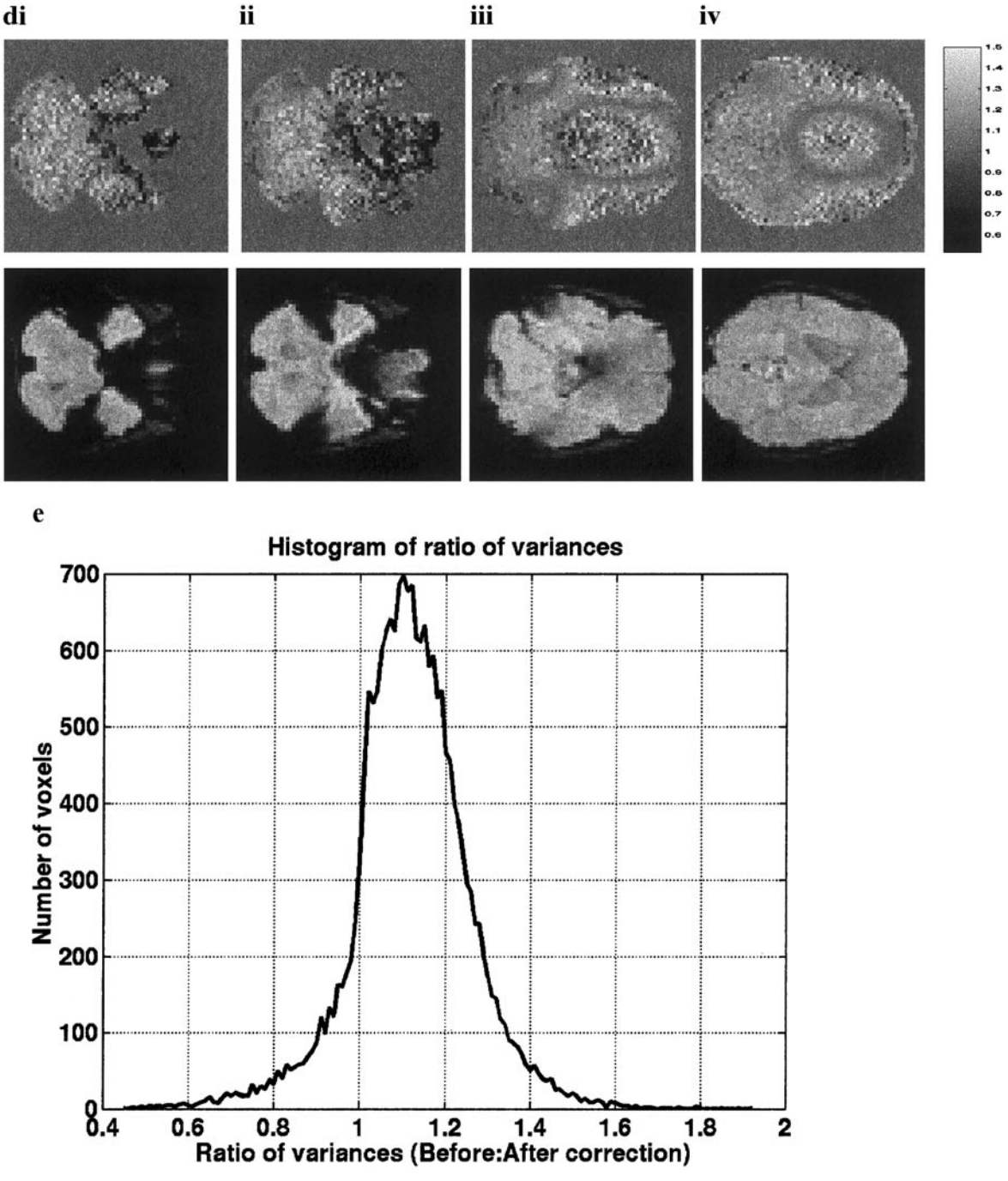

FIG. 5. Results for small movements. (a) Motion parameters for (i) rotation (about x-axis, blue; y-axis, green; z-axis, red) and (ii) translation (in x, blue; y, green; z, red). (b) Regions of the brain where distortion is significantly correlated with head motion. The overlaid statistics are thresholded at $P < 0.001$ (uncorrected for multiple comparisons). (c) Voxel timecourses through realigned residual field maps (scaled to represent voxel shifts). The dashed line shows a timecourse from a region where the magnetic field is nearly uniform and there is no correlation with head motion. The solid line shows a timecourse from a region where there is a significant correlation with head motion. (d) Slices from the quotient of the variance maps before and after distortion correction with the corresponding image slices in the bottom row. The grey-scale bar corresponds to the quotient values and the background of the image has been set to 1. Values >1 (brighter than the background) correspond to a decrease in variance due to distortion correction, values <1 (darker than the background) correspond to an increase in variance due to distortion correction and values $= 1$ correspond to no change in variance. (e) Histogram of quotient of variances.

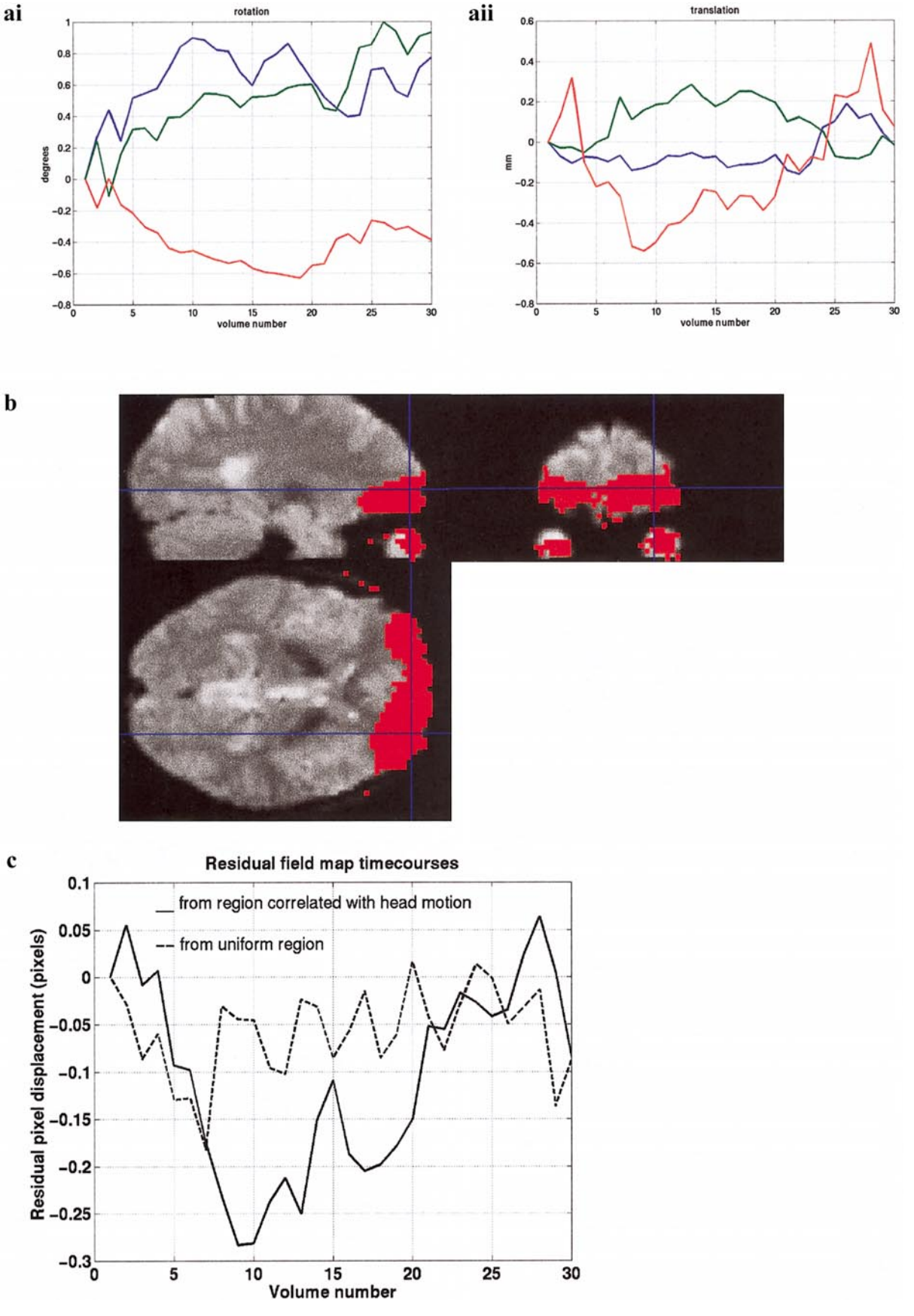

FIG. 6. Results for medium movements (as described in the legend of Fig. 5).

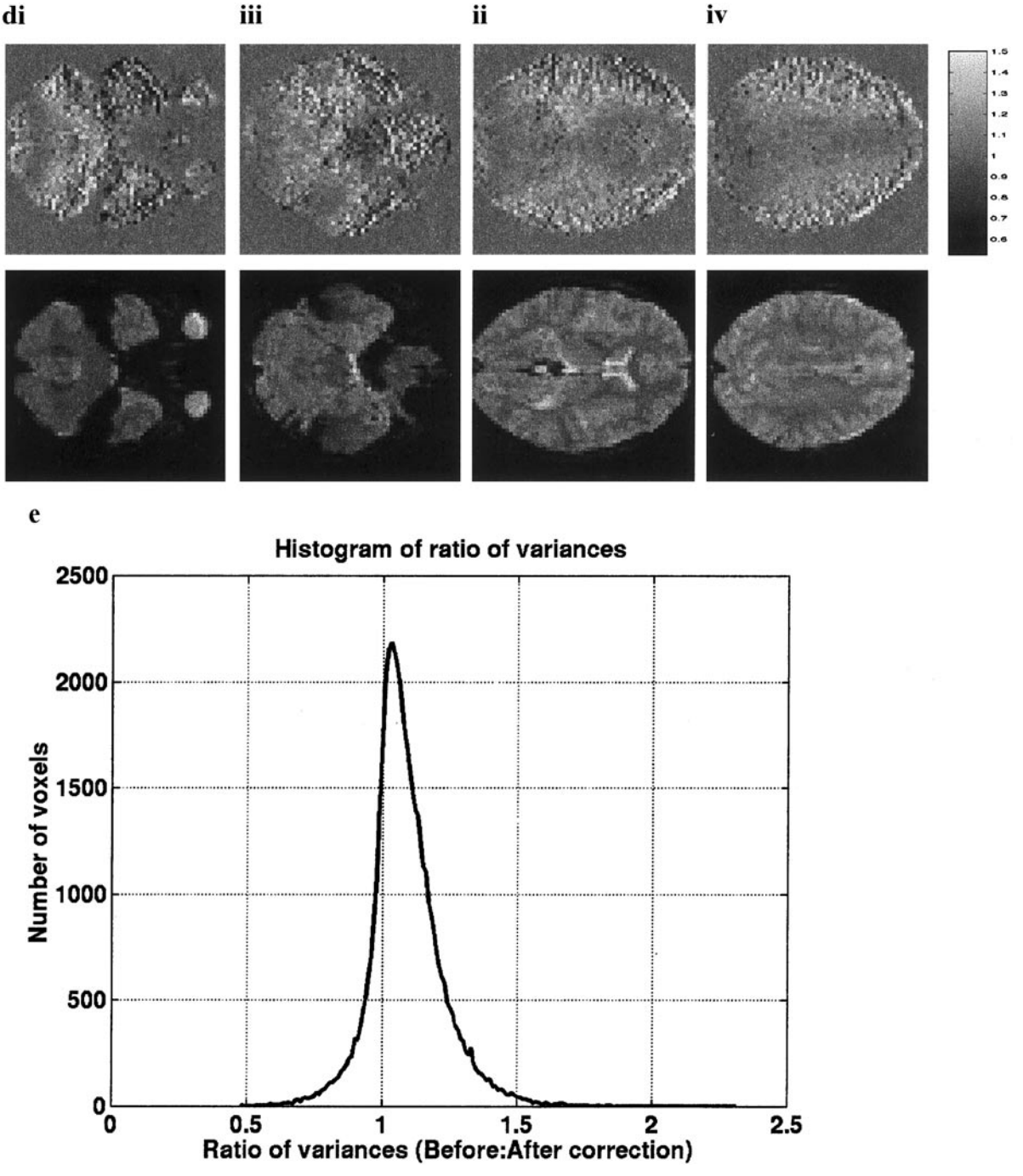

FIG. 6—*Continued*

Methods

Dual echo-time EPI images were acquired with the same parameters as described in the previous section. The images were acquired during short scanning sessions (about 3 min) for two different subjects. During each session the subject was first asked to keep as still as possible, then to move his head slightly and finally to move his head more. A field map was calculated from each pair of images in the time series and modeled by fitting DCT basis functions as described under "Creating a field map of the brain." A visual check was made to ensure that all field maps in the time series had been sensibly unwrapped and modelled. Each modeled field map was then used to correct for distortions in the corresponding image (the images with the longer echo-time (TE = 40 ms) were corrected). Intensity correction

was also applied to the distortion-corrected images as described by Eqs. (4) and (5).

Using SPM'99 the original image volumes were realigned to the first in the time series. The estimated motion parameters (three translations and three rotations) were then used to realign the field maps. A simple regression analysis was performed between the realigned field maps and the motion parameters to detect voxels for which the time courses in the realigned field maps were correlated with head movement. Movement correlated changes in the realigned field maps will correspond to time-varying changes in the distorted time-series. This analysis therefore identified regions in the brain where there was a significant interaction between head motion and geometric distortion. SPM'99 was used to create maps of F statistics to show the voxel-wise correlation between the field maps and the motion parameters. Voxels that survived a P value threshold of $P < 0.001$ (uncorrected for multiple comparisons) were considered to be significantly correlated with head motion. Our hypothesis was that brain regions affected by the interaction between distortion and head motion would be in areas where the constant component of the field inhomogeneity deviated most from zero (i.e., in areas most severely affected by susceptibility artefacts). These regions are near tissue boundaries where the field is most likely to vary as the head changes position.

The first field map in the time series was subtracted from the rest of the realigned field maps to generate a time series of residual field maps. Residual time courses were extracted from regions of the field map where (a) the magnetic field was nearly uniform and (b) there was a significant correlation with head motion. These time courses (in voxel displacements) were used to indicate the amplitude of the time-varying component of the field maps (i.e., the change in distortion due to motion).

Finally the images after distortion correction were realigned. The variance of each realigned image time series before and after distortion correction was calculated. A quotient of variance image was calculated for each pair of variance images, dividing the variance before by the variance after distortion correction. Where the quotient is greater than 1, the variance has been decreased by distortion correction and where the quotient is less than 1, the variance has been increased by distortion correction. Quotient values of 1 indicate no difference in the variance before and after distortion correction. A histogram of the quotient values was also constructed.

The data from the two subjects gave a range of different scales of head movements, which were then classified according to the scale of head motion. The classifications were small ($< \pm 0.2°$ and $< \pm 0.2$ mm), medium ($< \pm 1°$ and $< \pm 1$ mm) and large movements ($< \pm 5°$ and $< \pm 2.5$ mm). One set of results is shown for each range of movements.

Results

Results are shown from the first subject for small movements (Fig. 5) and for the second subject for medium and large movements (Figs. 6 and 7). These results do not represent all of the acquired data but are typical of the data classified with corresponding scales of movement.

For each of the quotient of variance maps (Figs. 5e, 6e, and 7e) there is a corresponding grey-scale bar. The background of each of the quotient of variance images has been set to 1. Therefore values >1 (brighter than the background) correspond to a decrease in variance due to distortion correction, values <1 (darker than the background) correspond to an increase in variance due to distortion correction and values = 1 correspond to no change in variance.

Small movements ($> \pm 0.2°$ and $< \pm 0.2$ mm—Fig. 5a). Less than 3% of voxels in the brain show a significant correlation with head motion (Fig. 5b). These voxels occur in the vicinity of the air-filled sinus in the inferior frontal region. They are mainly correlated with rotation about the x-axis and translation in the y- and z-axis.

The time course from a uniform region of the field map (Fig. 5c, dashed line) shows that residual voxel displacements vary by up to 0.12 voxels (0.36 mm). Similarly, the time course from the inferior frontal region (which is correlated with head motion, Fig. 5c, solid line) shows that residual voxel displacements vary by up to 0.15 voxels (0.45 mm).

Slices from the quotient of variance maps before and after distortion correction are shown in Figs. 5d (i–iv) together with the corresponding image slices. These illustrate that most voxels in the displayed slices have a value greater than 1 representing a global decrease in variance due to distortion correction. This is also evident in the histogram (Fig. 5e), which has a peak value at around 1.1. There are also regions where the distortion correction has increased the variance. This is evident in the region of the sinus (Figs. 5di and 5dii) and is probably due to the severe signal dropout and inaccuracies in the field map in this region. In Figs. 5diii and 5div there are contour shaped areas where the quotient of variance value is approximately equal to 1 (no change in variance). These regions correspond to zero crossings in the field maps where the field is relatively uniform and therefore distortion correction has not changed the images.

Medium movements ($< \pm 1°$ and $< \pm 0.6$ mm—Fig. 6a). Less than 4% of voxels in the brain show a significant correlation with head motion (Fig. 6b). These voxels occur in the frontal lobes and eyeballs. The timecourse from a uniform region of the field map (Fig.

6c, dashed line) shows that residual voxel displacements vary by nearly 0.2 voxels (0.6 mm). The time course from the frontal region (Fig. 6c, solid line) shows that residual voxel displacements vary by up to 0.3 voxels (0.9 mm). The realignment parameters illustrate that this time course is clearly correlated with translation in the z-axis (Figs. 6aii, red line).

Slices from the quotient of variance maps before and after distortion correction are shown in Figs. 6d (i–iv), together with the corresponding image slices. These illustrate that in all slices there are some regions of decreased variance (brighter voxels) away from the central regions of the brain. In particular the decrease in variance is illustrated by the bright region at the front edge of the brain corresponding to areas that are particularly vulnerable to distortion by movement effects. There are also some regions of increased variance due to distortion correction in regions affected by signal loss (i.e., dark voxels around the temporal lobes and sinuses in Figs. 6di and dii). The histogram of quotient values (Fig. 6e) has a peak at a value fractionally greater than 1, indicating that slightly more voxels show a decrease in variance due to distortion correction.

Large movements ($< \pm 5°$ and $< \pm 2.5$ mm—Fig. 7a). Around 10% of voxels in the brain show significant correlation with head motion (Fig. 7b). These voxels occur in a large portion of the frontal lobes and in the eyeballs. The timecourse from a uniform region of the field map (Fig. 7c, dashed line) shows that residual voxel displacements vary by up to 0.2 voxels (0.6 mm). The time course from the frontal region (Fig. 7c, solid line) shows that residual voxel displacements vary by up to 0.6 voxels (1.8 mm). The realignment parameters illustrate that this time course is clearly correlated with rotation about the x-axis (Fig. 7ai, blue line) and translation in the y- and z-axis (Fig. 7aii, green and red lines).

Slices from the quotient of the variance maps before and after distortion correction are shown in Fig. 7d (i–iv), together with the corresponding image slices. The pattern of decreases and increases in variance are similar to those in Fig. 6d. The edges of the brain (in particular at the front) show the greatest decrease in variance due to distortion correction. Around the middle of the brain there are regions where the quotient of the variance before and after distortion correction is approximately 1. This corresponds to uniform regions of the magnetic field where there is minimal distortion. Figures 7di and 7dii show regions of increased variance due to distortion correction, which as before correspond to regions affected by signal loss. Again, the histogram of quotient values (Fig. 7e) has a peak at a value fractionally greater than 1, indicating that slightly more voxels show a decrease in variance due to distortion correction.

In all of the results, the decrease in variance may be due to the smoothing effect of voxel resampling in the unwarping process in addition to the realignment and reslicing of the distortion corrected images. The results showed that even in uniform regions, the residual changes in the field maps were as large as 0.2 voxels (0.6 mm). These residual changes may be due to measurement noise or differences in the modeled field maps and may explain some of the increases in variance. Both increases and decreases in variance may also be caused by the intensity correction applied to correct for changes in voxel brightness. The aim of the intensity correction is to adjust intensity values that have been increased or decreased by distortion. However, the small local increases or decreases in intensity will correspond to small increases or decreases in variance with respect to the original images. A more thorough assessment of the positive and negative effects of intensity correction would be an interesting avenue for further work. In a comparison of different unwarping methods using regularised B0 maps (Jenkinson, 2001), intensity correction was not shown to improve the distortion correction.

DISCUSSION

In this paper we have assessed the effect of image distortion correction for fMRI at 2T. This field mapping method of distortion correction is well understood, and relatively quick and simple to implement. We have explored how this method can be optimized to acquire robust field maps, investigated field map smoothing and have quantified the effect of distortion correction on anatomical coregistration. We have also investigated whether the field mapping technique can be used to correct for the interaction between geometric distortion and head motion in fMRI time series.

Field Map Acquisition and Calculation

We have shown that a dual echo-time EPI sequence can be used to acquire and calculate robust field maps. Using this fMRI sequence to acquire the field map data means that the field map and the fMRI data will share the same geometric properties. The field map will therefore provide an accurate representation of the voxel shifts that can be applied with minimal processing to fMRI data. The longer echo-time of the dual echo-time sequence should be equal to that used for fMRI scanning. This echo-time is usually chosen to optimise the sensitivity of detection of BOLD signal, i.e., the echo-time is approximately equal to the T2* of grey matter at a particular field strength (Bandettini *et al.*, 1994). The shorter echo time should be chosen so that the echo-time difference is long to minimise field map noise but short enough to allow robust phase unwrapping. We have found an echo time offset of around 10 to 15 ms to be appropriate in this work.

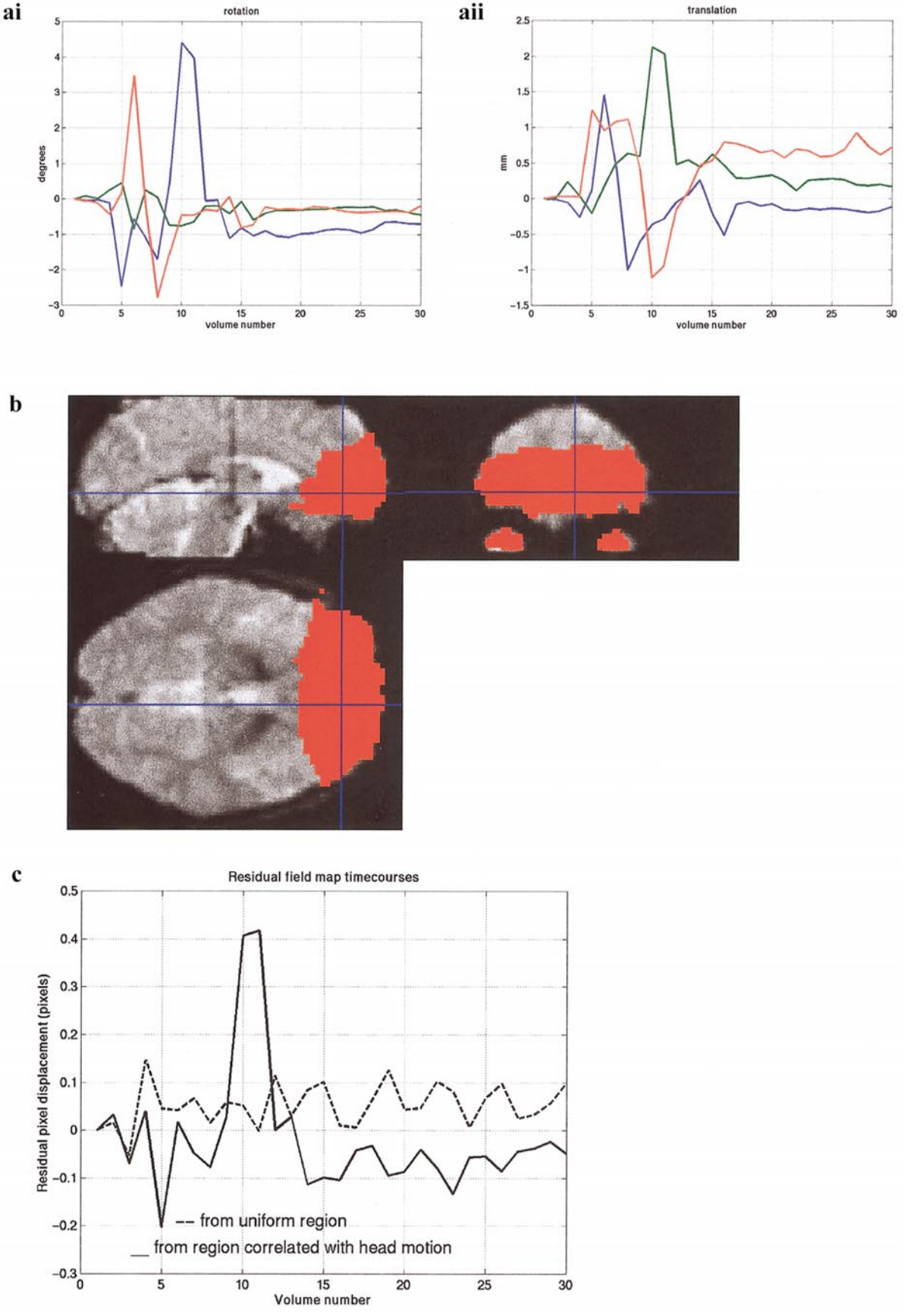

FIG. 7. Results for large movements (as described in the legend of Fig. 5).

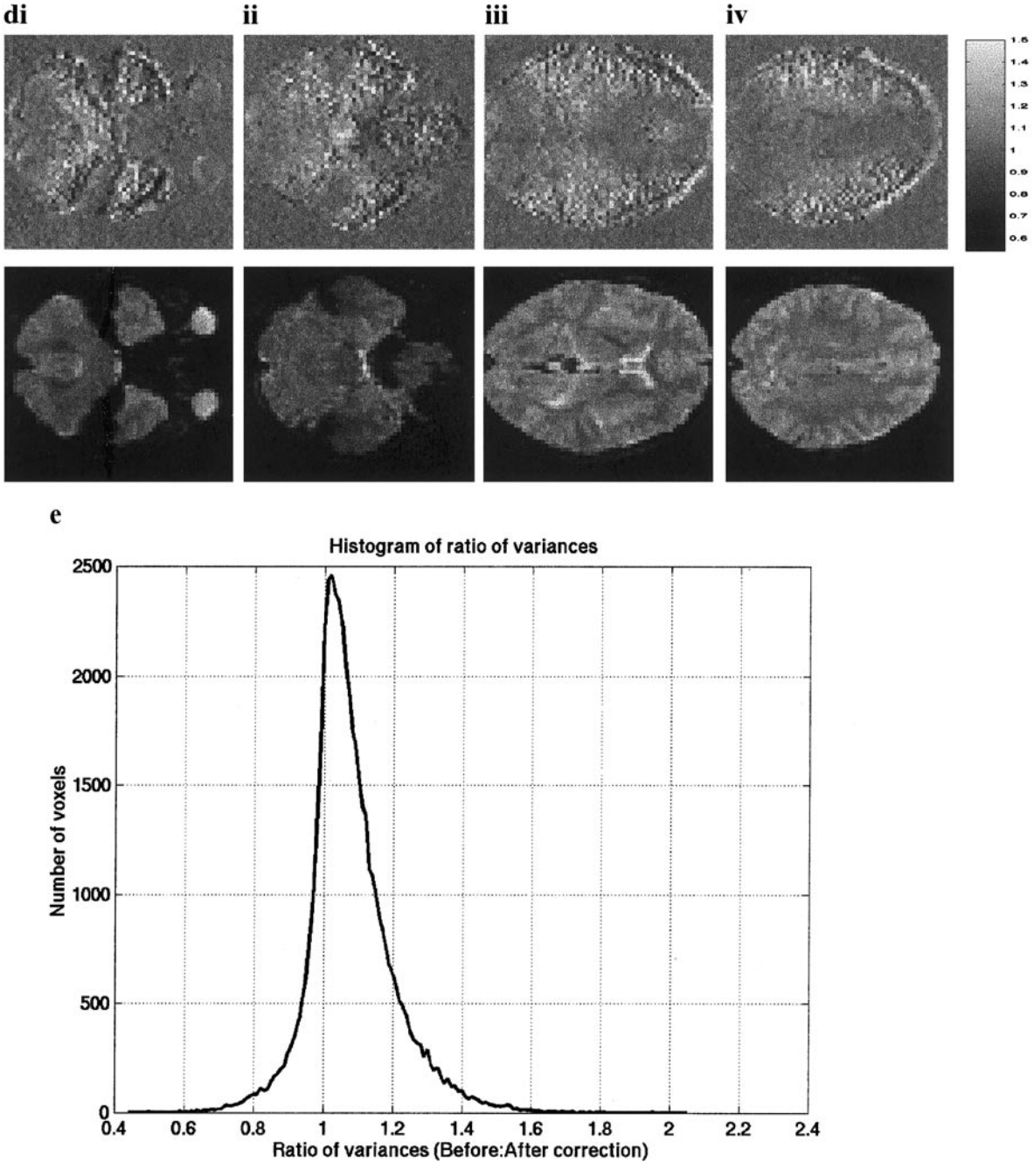

FIG. 7—*Continued*

The main disadvantage of using an EPI sequence to acquire the field maps is that because the field map is acquired in distorted space, in regions where voxel compression is greatest, there is minimal information available for the distortion correction. In these regions, we rely on interpolation to fill in the missing intensity values.

We have shown that a smoothed field map (using gaussian smoothing or fitting a DCT basis function model) decreases the noise that may otherwise introduce spatial inaccuracies into the distortion corrected images. By constructing a low-noise mean field map we have also shown that too much smoothing can have an artifactual blurring effect in regions of the brain where there are large susceptibility artefacts and the field changes rapidly. In these regions, the accuracy of the distortion correction may be reduced. With a small amount of gaussian smoothing (FWHM = 1 voxel) there is less than a fraction of a voxel deviation from the true field map in regions where the field changes

rapidly. However, such a small amount of smoothing will be less effective in decreasing noise or field map errors so that optimising the field map acquisition is more important.

Artifactual blurring is more extreme when fitting a basis function model to the field map. Fitting the basis function model requires that the true field inhomogeneity is a smoothly varying function over all regions of the brain. This assumption is most violated at boundaries between regions with different susceptibilities. In these regions the fitted field map can deviate from the true field map by up to a voxel. However, it must be pointed out that these regions are usually associated with signal loss in the image so that inaccuracies in the distortion correction are less important. The advantage of fitting a smooth function to the original field map is that it allows the field to be described parametrically and can therefore be estimated in regions of the brain where it can not be measured accurately. The problem of reducing noise without artifactual blurring may be resolved using an anisotropic smoothing method such as anisotropic diffusion (Perona and Malik, 1990). This method encourages smoothing within homogeneous regions in preference to smoothing between regions and is therefore more likely to preserve the boundaries between tissues with different susceptibilities.

Distortion Correction and Anatomical Coregistration

Other authors have validated the field mapping technique for distortion correction using phantoms (Jezzard and Balaban, 1995). The aim of this work was to investigate in vivo the effect of geometric distortion on anatomical coregistration and determine whether the mismatch between anatomical images and EPI data could be minimised using the field mapping method for distortion correction. The results of this work show that at 2T, geometric distortions of the order of 1 to 1.5 voxels are clearly visible when comparing EPI data (before and after distortion correction) with the coregistered anatomical data. Distortions of this size correspond to the voxel shifts calculated from the field maps. The field maps also show larger distortions (of the order of 2–3 voxels) in the inferior frontal and temporal regions of the lower slices of the brain where susceptibility artefacts are most severe. However, signal loss in these regions makes a visual assessment of both the distortion correction and the anatomical coregistration difficult.

We used a linear coregistration method based on mutual information that provides a quantitative measure (the entropy correlation coefficient) to determine whether the distorted or the undistorted images better match the anatomical image. We compared no distortion correction with four different methods of distortion correction, using a gaussian smoothed field map, a modeled field map, both with and without intensity correction. Overall, the coregistration results were improved for all methods of distortion correction. We therefore propose that if distortion correction has been applied it is possible to find a better match between EPI and anatomical images using a linear coregistration method.

No single distortion correction method gave a consistently better match for all of the data sets acquired in this work. In the experiment using the low-noise mean field map, the modelled field map resulted in a less accurate representation of the true field in regions where the field changes rapidly. However, it should also be noted that these regions correspond with regions of signal loss and are less likely to influence the results of a coregistration method based on mutual information. The distortion correction with intensity correction improved the coregistration results in just 1 subject. One would imagine that a correction for artifactual increases and decreases in image intensity would improve anatomical coregistration. However further work is required to fully assess the impact of such an adjustment for intensity.

An alternative approach for anatomical coregistration involves determining the non-linear transformation that warps a distorted image to match the anatomical image (Studholme *et al.*, 2000). However, in regions of signal loss, it may not be possible to calculate the local non-linear distortion required for an accurate coregistration.

The scale of geometric distortions seen in our EPI data acquired at 2T may not be detrimental to group studies where data is spatially normalised and the spatial distances between functional activations may be of the order of a few millimeters. However a more accurate registration is required when precise spatial localisation is necessary, for example in single subject studies or when anatomical information is used as a spatial reference to sample the functional data (e.g., cortical surface analyses). The method of field mapping for distortion correction can provide robust information about geometric distortions in most regions of the brain and can be used to improve anatomical coregistration.

Distortion Correction and Head Motion

In this work we used a dual echo-time EPI sequence to calculate a unique field map at each time point in an fMRI time series. This allowed us to characterise and evaluate residual variations caused by the interaction between geometric distortion and head motion. In our data the constant component of the field maps has geometric distortions of up to 2–3 voxels (6–9 mm). Distortions of this order only exist in brain regions where there are severe susceptibility artefacts. In these regions, the size of residual variations in distortion (varying with head motion) increases from 0.15 voxels (0.45 mm) up to nearly 0.5 voxels (1.5 mm) as the scale of head movement increases.

For the small movement data, the residual variations in the field maps are of the same order in uniform as well as non-uniform regions of the field (<0.15 voxels, 0.45 mm). Temporal noise or differences between successively measured and modeled field maps may cause this scale of residual variations in the small movement data. In this data, fewer than 3% of the total number of voxels in the brain are significantly correlated with motion parameters and these voxels are localised in the vicinity of the air-filled sinus in the inferior frontal region. In the same region, distortion correction introduced additional variance into the time series. This is probably because the low signal-to-noise ratio (caused by susceptibility artefacts) makes the data very sensitive to any temporal noise introduced by applying a unique distortion correction to each image in the time series.

When the scale of the head motion is larger, less of the variance in the time series can be explained by the application of a unique distortion correction to each image in the time series. The two time series involving larger head motion show that the interaction between residual distortions and head movement occurs in more extensive regions of the brain mainly eyeballs, frontal and some temporal regions. The residual variations in the field maps can be up to 0.5 voxels (1.5 mm) for larger movements (<5° rotation and <2.5 mm). It is important to be aware of the regions that may be affected by this movement-distortion interaction because it could lead to false positives if the experimental task is at all correlated with head movement.

In all of the results, there is a small global decrease in variance after applying the distortion correction. This may be due to the smoothing effect of voxel resampling and interpolation in the distortion correction step followed by the additional realignment. The smoothing effect of linear interpolation is equivalent to convolution with a triangular function, FWHM = 1 voxel. However, this is only the approximate smoothing effect of the distortion correction since different voxels are resampled at different subvoxel positions. The additional intensity correction applied to adjust local changes in voxel brightness may be able to improve the estimation of motion parameters. However, it also changes the noise structure and introduces some small local increases and decreases in variance.

The estimation of realignment parameters may be effected by the interaction between head movement and distortions, especially for larger head movements. However, additional variance or temporal noise introduced by distortion correction using successive field maps may also effect the estimation of realignment parameters. Ideally, the unwarping process and the application of the linear transformation to realign the images should be carried out simultaneously (e.g., Andersson *et al.*, 2001).

A field map can provide information about the static component of geometric distortion and be used to correct for distortions in EPI providing an improved match with anatomical images. Residual time-varying geometric distortions can be characterised using a dual echo-time sequence to calculate a unique field map at each time point. However, it seems that there is too much variability between successive field maps to use this method to correct for time-varying distortions. These results suggest that the distortion correction of time-series must be temporally and spatially smooth without compromising accuracy in regions where the magnetic field changes rapidly and the distortions are largest. The correction of time-varying geometric distortions may benefit from methods that attempt to estimate the distortions from the images and their derivatives with respect to head position (e.g., see Andersson *et al.* (2001)).

ACKNOWLEDGMENT

This work was funded by The Wellcome Trust.

REFERENCES

Andersson, J., Hutton C., Ashburner, J., Turner, R., and Friston, K. 2001. Modelling geometric deformations in EPI time series. *Neuroimage* **13:** 903–919.

Andrade, A., Kherif, K., Mangin, J-F., Worsley, K. J., Simon, O., Dahaene, S., Le Bihan, D., and Poline, J-B. 2000. Cortical surface statistical parametric mapping. *NeuroImage* **11:** S504.

Axel and Morton. 1989. Correction of phase wrapping in magnetic resonance imaging. *Med. Phys.* **16**(2): 284–287.

Bandettini, P. A., Wong, E. C., Jesmanowicz, A., Hinks, R. S., and Hyde, J. S. 1994. Spin-echo and gradient-echo EPI of human brain activation using BOLD contrast: A comparative study at 1.5T. *NMR Biomed.* **7:** 12–20.

Bowtell, R., McIntyre, D. J. O., Commandre, M-J., Glover, P. M., and Mansfield, P. 1994. Correction of geometric distortion in echo planar images. *Soc. Magn. Res. Abstr.* **2:** 411.

Chen, N-K., and Wyrwicz A. M. 1999. Correction for EPI distortions using multi-echo gradient-echo imaging. *Magn. Reson. Med.* **41:** 1206–1213.

Collignon, A., Maes, F., Delaere, D., Vandermeulen, D., Suetens, P., and Marchal, G. 1995. Automated multi-modality image registration based on information theory. In *Proceedings of Information Processing in Medical Imaging* (Y. Bizais *et al.*, Eds.) Kluwer Academic Publishers.

Cusack, R., Huntley, J. M., and Goldrein, H. T. 1995. Improved noise-immune phase-unwrapping algorithm. *Appl. Optics* **34**(5): 781–789.

Cusack, R., Papdakis, N., Martin, K., and Brett, M. 2001. A new robust 3d phase-unwrapping algorithm applied to fMRI field maps for the undistortion of EPIs. *NeuroImage* **13:** S103.

Deichmann, R., Good, C. D., Josephs, O., Ashburner, J., and Turner, R. 2000. Optimization of 3-D MP-RAGE sequences for structural brain imaging. *NeuroImage* **12:** 112–127.

Devlin, J. T., Russell, R. P., Davis, M. H., Price, C. J., Wilson, J., Moss, H. E., Matthews, P. M., and Tyler, L. K. 2000. Susceptibility-induced loss of signal: Comparing PET and fMRI on a semantic task. *Neuroimage* **11:** 589–600.

Fischl, B., Sereno, M. I., and Dale, A. M. 1999. Cortical surface-based analysis II: Inflation, flattening, and a surface-based coordinate system. *NeuroImage* **9:** 195–207.

Gorno-Tempini, M. L., Hutton, C., Josephs, O., Deichmann, R., Price, C., and Turner, R. 2001. Echo time dependence of BOLD contrast and susceptibility artifacts. *NeuroImage* **15:** 136–142.

Hedly, M., and Rosenfeld, D. 1992. A new two-dimensional phase unwrapping algorithm for MRI images. *Magn. Reson. Med.* **24:** 177–181.

Jain, N. K. 1989. In *Fundamentals of Digital Image Processing*, pp. 150–154. Prentice Hall, Englewood Cliffs.

Jenkinson, M. 2001. Improved unwarping of EPI images using regularised B0 maps. *Neuroimage* **13:** S165.

Jesmanowicz, A., Biswal, B. B., and Hyde, J. S. 1999. Reduction in GR-EPI intravoxel dephasing using thin slices and short TE. *Proc. Int. Soc. Magn. Reson. Med.* P. 1619.

Jezzard, P., and Balaban, R. S. 1995. Correction for geometric distortion in echo planar images from Bo field variations. *Magn. Reson. Med.* **34:** 65–73.

Jezzard, P., and Clare, S. 1999. Sources of distortion in functional MRI data. *Hum. Brain. Mapp.* **8:** 80–5.

Josephs, O., Deichmann, R., and Turner, R. 2000. Trajectory measurement and generalised reconstruction in rectilinear EPI. *NeuroImage* **11:** S543.

Maes, F., Collignon, A., Vandermeulen, D., Marchal, G., and Suetens, P. 1997. Multimodality image registration by maximisation of mutual information. *IEEE Trans. Med. Imag.* **16**(2): 187–198.

Mao, H., and Kidambi, S., 2000. Reduced susceptibility artefacts in BOLD fMRI using localised shimming. *NeuroImage* **11:** S553.

Matlab 5.3.1. 1999. The Math Works, Inc. copyright 1984–1999. Natick, MA. (http://www.mathworks.com/)

Ojemann, J. G., Akbudak, E., Snyder, A. Z., McKinstry, R. C., Raichle, M. E., and Conturo., T. E. 1997. Anatomic localisation and quantitative analysis of gradient refocused echo-planar fMRI susceptibility artefacts. *Neuroimage* **6:** 156–167.

Perona, P., Malik, J. 1990. Scale-space and edge detection using anisotropic diffusion. *IEEE Trans. Pattern Anal. Machine Intell.* **12:** 629–639.

Reber, P. J., Wong, P. J., Buxton, R. B., and Frank, L. R. 1998. Correction of off resonance-related distortion in echo-planar imaging using EPI-based field maps. *Magn. Reson. Med.* **39:** 328–330.

Schmitt, F., Stehling, M. K., and Turner, R. 1998. *Echo-Planar Imaging: Theory and Application*. Springer-Verlag, Berlin/Heidelberg.

Studholme, C., Constable, R. T., and Duncan, J. S., 2000. Accurate alignment of functional EPI data to anatomical MRI using a physics based distortion model. *IEEE Trans. Med. Imaging* **19:** 1115–1127.

Van Essen, D. C., and Drury, H. A. 1997. Structural and functional analyses of human cerebral cortex using a surface-based atlas. *J. Neurosci.* **17:** 7079–7102.

Wan, X., Gullberg, G. T., and Parker, D. L. 1995. Reduction of geometric distortion in echo-planar imaging using a multi-reference scan. *Soc. Magn. Res. Abstr.* **3:** 103.

Weisskoff, R. M., and Davis, T. L. 1992. Correcting gross distortion on echo planar images. *Soc. Magn. Res. Abstr.* **11:** 4515.